Bulletin 145

New Mexico Bureau of Mines & Mineral Resources

A DIVISION OF
NEW MEXICO INSTITUTE OF MINING & TECHNOLOGY

Late Mesozoic to Cenozoic cooling histories of the flanks of the northern and central Rio Grande rift, Colorado and New Mexico

Shari A. Kelley[1], Charles E. Chapin[2], and Jeff Corrigan[3]

[1]Department of Geological Sciences, Southern Methodist University, Dallas, Texas 75275; [2]New Mexico Bureau of Mines & Mineral Resources, Socorro, New Mexico 87801; [3]ARCO Oil and Gas Company, Plano, Texas 75075

SOCORRO 1992

Original Printing

Published by Authority of State of New Mexico, NMSA 1953 Sec. 63-1-4
Printed by University of New Mexico Printing Services, December 1992

Available from New Mexico Bureau of Mines & Mineral Resources, Socorro, NM 87801

Contents

Figures

Tables

Abstract

Apatite fission-track (FT) data collected in the northern and central Rio Grande rift of New Mexico and Colorado indicate that rocks now exposed in the eastern and western margins of the rift cooled during uplift and erosion in a complex spatial and temporal pattern. FT data from the Santa Fe Range, Los Pinos Mountains, and northern Nacimiento Mountains indicate that these mountain blocks cooled during the early stage of the Laramide orogenic event. Other mountain blocks (southern Nacimiento and Manzano Mountains, high elevation portions of the Sangre de Cristo Mountains and Magdalena Mountains) began cooling during the late stage of the Laramide event and subsequent Eocene erosion. The Sandia Mountains, Blanca Peak, Joyita Hills, Sierra Ladrones, the high-elevation portion of the Sawatch Range, and the lower-elevation samples in the Sangre de Cristo Mountains began cooling during early extension of the Rio Grande rift and/or waning of regional volcanism in the late Oligocene and early Miocene. The eastern front of the Sawatch Range, the Sangre de Cristo Mountains north of Blanca Peak, the low-elevation portion of the Sangre de Cristo Mountains near San Luis, Colorado, and the Lemitar Mountains cooled during late-stage rifting in middle to late Miocene. Generally, the youngest FT ages are found in the rift flanks adjacent to large normal faults along the deep margins of the en-echelon half-grabens that make up the present Rio Grande rift. Two of the blocks with Miocene FT ages, the Sierra Ladrones and Blanca Peak, are promontories that project into rift basins at the junction of arcuate normal faults bounding the deep side of half-grabens. Tectonic denudation of three sides has allowed unusually rapid isostatic uplift in these blocks. Similarly, the Sangre de Cristo Mountains north of Blanca Peak are bounded on two sides by active late Cenozoic faults that have allowed the rapid isostatic rise of these mountains. Cooling rates increased from the Laramide orogenic event (1 to 4°C/Ma) to the development of the Rio Grande rift (7 to 20°C/Ma).

Introduction

The Southern Rocky Mountains in Colorado and New Mexico have had a long and complex geologic history, culminating in the Late Cretaceous (Campanian and Maastrichtian) to late Eocene with the compressional Laramide orogenic event. A widespread surface of low relief was carved across much of the area in late Eocene (Epis and Chapin, 1975). Major volcanism affected the province during the Oligocene (Lipman, 1975). The Rio Grande rift, an extensional feature that bisects the Southern Rocky Mountains, began to form about 30 Ma and developed during two phases of regional extension (Chapin and Seager, 1975; Morgan et al., 1986; Aldrich et al., 1986). The early (30 to 18 Ma) northeast—southwest-oriented phase of extension is characterized by the development of broad, shallow basins, low-amplitude topographic relief, local areas of intense extension associated with low-angle normal faults, and the emplacement of large volumes of silicic ash-flow tuffs and basaltic andesite lavas. The later phase of extension (primarily 10 to 5 Ma) is characterized by the development of deep half-grabens, high topographic relief, the formation of widely spaced, high-angle normal faults, and the emplacement of alkali-olivine and tholeiitic basalts (Chapin and Seager, 1975; Morgan et al., 1986).

The tectonic development of Southern Rocky Mountains in the vicinity of the rift has been determined primarily by studying the depositional and structural history of sedimentary and volcanic rocks preserved in and adjacent to the rift basins. Two of the basins of the northern Rio Grande rift, the San Luis Basin and the Albuquerque—Belen Basin, are largely undissected so that the early history in these basins is not well constrained, although data from seismic lines and petroleum test wells have improved the understanding of these areas in recent years (Brister and Gries, 1992; Lozinsky, 1988; Russell and Snelson, 1990). Little has been done to estimate the uplift rate or timing of uplift of the mountain ranges that bound the margins of the rift. Many of the rift models in the literature predict uplift rates, but there are few data to test these predictions. Fission-track (FT) data from rocks exposed along the flanks of the rift provide powerful constraints for these models.

The principal objectives of this paper are: (1) to present new apatite fission-track ages for rocks exposed in the uplifts along the eastern and western margins of the northern and central Rio Grande rift (Fig. 1); (2) to use the FT data to discuss the local tectonic and cooling history of each mountain block investigated; (3) to integrate the FT data from all the mountain ranges into a discussion of the tectonic development of this region during Laramide compression, mid-Tertiary magmatism, and Rio Grande rift extension; (4) to use the FT results to qualitatively assess tectonic models that have been proposed to explain uplift of the flanks of the Rio Grande rift.

Interpretation of fission-track data

Consider a rock volume that cools from high temperatures during uplift and erosion. Fission tracks in apatite in the rock are produced at a constant rate due to the spontaneous fission decay of ^{238}U and are annealed at a rate controlled by the temperature. As cooling begins, the fission-track annealing rate is greater than the production rate and no tracks accumulate in the apatite. As cooling proceeds, the apatite passes through a temperature range known as the zone of partial stability (60 to 140°C) where partially annealed tracks are retained. Finally, at low temperatures, fission tracks that are produced are retained and annealing is relatively minor. The partially annealed and nearly fully retained tracks are all used to calculate an apparent age. The fission-track method "dates" the cooling of a rock through the closure temperature of approximately 100°C; it should be noted that the method does not necessarily date a discrete cooling event, but the "age" represents an interval of time. The length of this time interval is dependent on the cooling rate.

Denudation rates from apparent fission-track ages

A simple method of determining approximate timing and rates of cooling due to uplift and erosion is based on the measurement of apatite fission-track ages as a function of elevation in a mountain range. Since rocks at higher present-day elevations cooled before rocks at lower present-day elevations, the apparent ages at higher elevations will be older. The ages at high elevation can be used as a minimum estimate of the initiation of denudation, and the difference in ages at the higher and lower elevations can be used to calculate apparent denudation rates. The denudation rate can be derived from the apparent denudation rate only when: (1) the 100°C isotherm is horizontal during denudation; (2) the distance between the surface and the 100°C isotherm remains constant as denudation occurs (i.e. constant geothermal gradient); (3) uplift equals erosion (Parrish, 1983). These assumptions are not always met, particularly in an area with a complicated tectonic history like the Rio Grande rift.

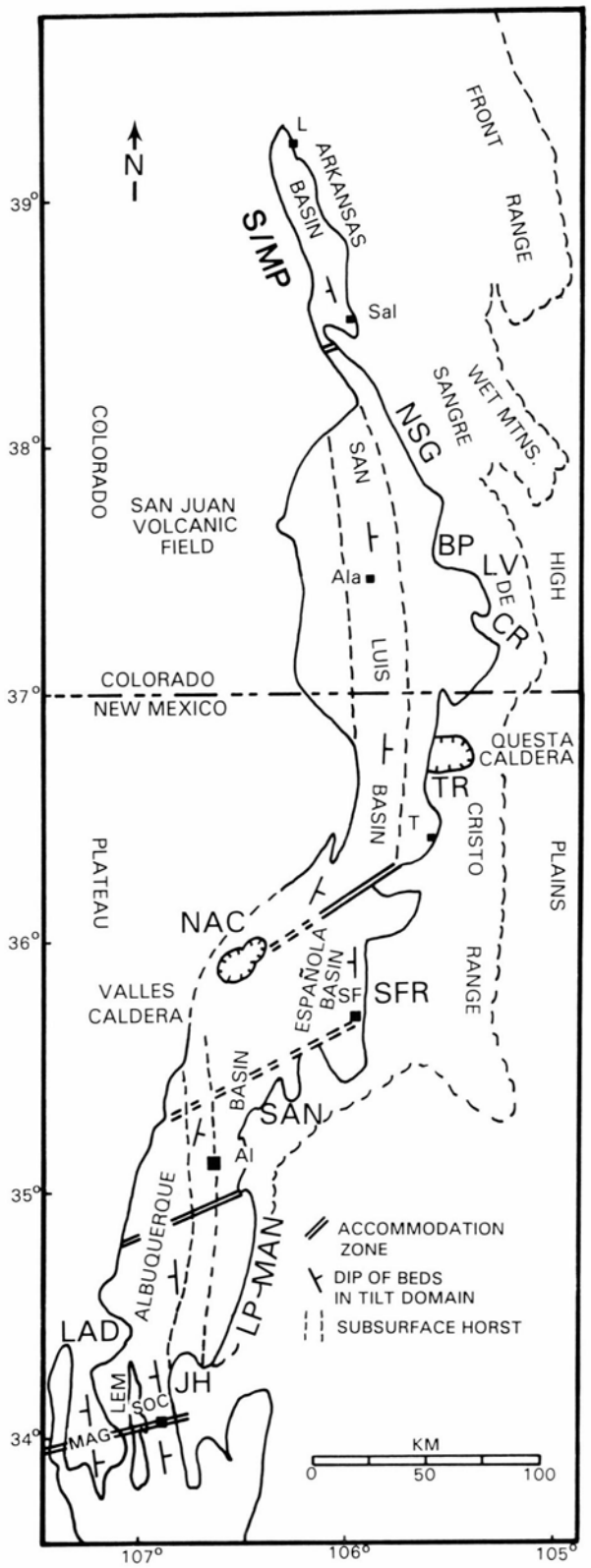

FIGURE 1—Regional location map for the northern and central Rio Grande rift. The mountain ranges discussed in this paper are designated by bold capital letters: S/MP = Sawatch Range/Mt. Princeton batholith, NSG = northern Sangre de Cristo Mountains, BP = Peak, LV = La Veta Pass, CR = Culebra Range, TR = Taos Range, SFR = Santa Fe Range, NAC = Sierra Nacimiento, SAN = Sandia Mountains, MAN = Manzano Mountains, LP = Los Pinos Mountains, JH = Joyita Hills, LAD = Sierra Ladrones, LEM = Lemitar Mountains, MAG = Magdalena Mountains. Cities and towns shown for reference are: L = Leadville, Sal = Salida, Ala = Alamosa, T = Taos, SF = Santa Fe, Al = Albuquerque, and SOC = Socorro. Base map after Chapin (1988).

A better approach to determining the cooling history of a mountain block involves using confined track-length measurements in combination with the apparent ages. The shape of confined track-length distributions provides useful information about cooling history (Gleadow et al., 1986). For example, a sample with a simple cooling history would have a unimodal track-length distribution, with short tracks forming as the apatite cools through the zone of partial stability, and longer tracks (14 to 18 **p.m)** forming after the mineral cools to temperatures where the tracks are largely retained. If the rock cools slowly (1 to 5°C/Ma), the peak of the track-length distribution is skewed toward longer tracks. If the sample cools rapidly (5 to <10°C/Ma), the track-length distribution is relatively symmetrical about long tracks. Finally, if a rock cools very slowly (<1°C/Ma), so that it remains in the zone of partial stability for a long time, the histogram is broad and multimodal. Green et al. (1989) described how length and age data can be used to quantitatively determine the thermal history experienced by a sample. The cooling histories determined by fission-track analysis (Green et al., 1989) from a set of samples collected along a traverse through a mountain range can potentially be used to determine denudation rates, assuming reasonable estimates of geothermal gradient during denudation can be established.

Procedures

One hundred and forty samples of Proterozoic igneous and metamorphic rocks, Paleozoic to Mesozoic sedimentary rocks, and Eocene to Oligocene plutonic rocks were collected along traverses through ranges that flank the margins of the Rio Grande rift (Fig. 1). The criteria used in locating the traverses included the occurrence of significant vertical relief and the presence of rock types containing adequate amounts of apatite for FT dating. Elevations of the samples were determined from U.S. Geological Survey 1:24,000 scale topographic maps to an estimated accuracy of ± 6 m.

Apatite was separated from the samples using standard heavy liquid (sodium polytungstate with a density of 2.95 gm/cm^3 and methylene iodide) and magnetic-separation techniques. One hundred and ten samples containing sufficient apatite were prepared for FT dating by the external detector method (EDM) (Naeser, 1979).

Apatite grains were mounted in an epoxy wafer, polished to expose the grains, and etched for 25 seconds in a 5 M solution of nitric acid to reveal the fission tracks. The apatite-grain mounts were then covered with muscovite detectors and sent to the Texas A&M Nuclear Science Center for irradiation. The muscovite-detector records induced tracks produced by the fission of 'U during bombardment of the samples with thermal neutrons in the reactor. The neutron flux was calibrated with Durango and Fish Canyon age standards, NBS SRM glass 962, and Corning Glasses CN-5 and CN-6. A zeta value (Hurford and Green, 1983) of 351
± 40 was determined using the NBS glass and the accepted ages of 27.9 ± 0.7 Ma for the Fish Canyon Tuff and 31.4
± 0.5 for Durango apatite (Green, 1985).

Upon return from the reactor, each muscovite detector was removed from the grain mount and etched in 48% hydrofluoric acid for 13 minutes in order to reveal induced fission tracks. The muscovite detectors from the glass standards and the age standards were etched in hydrofluoric acid for 45 minutes and 13 minutes, respectively. Twenty apatite grains were examined in each sample, when possible.

Calculation of fission-track ages and error statistics

Individual-grain ages were calculated using the methods described by Naeser (1979) and Hurford and Green (1983). The Chi-squared statistic (Galbraith, 1981) is used to determine whether the individual ages belong to a single pop-

ulation. Mixed ages caused by partial annealing, variations in sediment provenance, or sample contamination are indicated when the Chi-squared statistic does not pass at the 5% probability level. If the individual-grain ages pass the Chi-squared test, then a conventional age estimate using the sum of the spontaneous and induced counts for all the grains is calculated, and the errors in the age are computed using the methods of Galbraith and Laslett (1985). The conventional age estimate is not valid for samples with mixed ages because there is a bias toward grains with higher track densities. In cases where the sample fails the Chi-squared test, the mean grain age is more appropriate, since the failure indicates that the variation is greater than that due to Poisson counting error; a Gaussian component may be present. In this study, all of the samples except 88NAC13 and 88NAC15 passed the Chi-squared test. The samples that failed the test are both sandstones. The failure is the result of the diverse provenance of the apatite grains in the sandstones; a mean fission-track age is reported for these samples.

Fission-track length measurements

The confined track-length distributions in the apatite-grain mounts were determined using a microscope fitted with a 100-x oil immersion lens, a drawing tube, and a digitizing tablet. The system allows the track lengths to be measured to approximately ± 0.2 µm. Horizontal, well-etched, confined tracks (tracks completely enclosed within the crystal) in grains with prismatic faces were measured. The orientation of the tracks with respect to the c-axis was also measured.

Microprobe analyses

Green et al. (1986) found that fission tracks in chlorine-rich detrital apatite anneal more slowly than tracks in fluor-apatite. Consequently, within a sedimentary rock containing apatite from several sources, the older individual-grain ages tend to be associated with grains of chlorine-rich apatite.

Apatites from many of the crystalline and sedimentary rocks in this study were analyzed using an electron microprobe. Two ideas were tested. First, we wanted to determine if there is a correlation between mineral chemistry and individual-grain age, particularly in the sedimentary rocks. Second, we wanted to determine if there is a correlation between the overall mineral chemistry of each sample and the pooled age for the sample in an attempt to identify chemical versus thermal controls on the ages of these geographically scattered samples.

The grains were analyzed with an electron-beam accelerating voltage of 15 kV and a beam current of 15 nA. Apatite (Durango) and scapolite (Smithsonian Std. R6600) were used to calibrate the fluorine and chlorine peaks, respectively. When possible, the dated grains were probed twice, once in the center and once on the rim, to test for zoning. No zoning was observed in these samples. The chlorine content of each grain is based on a $Ca10(PO4)6(F, OH, C1)_2$ molecule. For reference, Durango apatite has 0.4 wt% Cl.

Time—temperature estimates

Recently, the significance of the thermal-history information contained in track-length distributions has been recognized, and the process of fission-track annealing in apatite has been empirically calibrated in the laboratory (Laslett et al., 1987; Duddy et al., 1988; Green, 1988; Green et al., 1989; Crowley et al., 1991). Using published laboratory results, Corrigan (1991) developed an inversion algorithm that utilizes the conventional age and track-length distribution of a sample to quantitatively extract time—temperature information recorded in apatite. The algorithm uses an annealing model developed by Carlson (1990). The values of A, Q, and n used in this investigation are the composite parameters of Carlson (1990) derived from the combined data sets of Green et al. (1986) and Donelick (1988).

The forward problem is quite nonlinear and it is difficult to find a unique solution. Corrigan's (1991) approach involves finding thermal histories that satisfy the FT age, length distribution, and present temperature data using an optimization procedure known as simulated annealing. Two assumptions form the basis of this analysis. First, the chemical composition of the apatite should vary over a small range. Second, the equations of Carlson (1990), which are in a mathematical form well-suited to the simulated annealing procedure, are assumed to accurately depict the evolution of track-length reduction along a given time—temperature path. The process of fission-track annealing is not completely understood and alternative annealing equations have been proposed (Laslett et al., 1987; Crowley et al., 1991). Two recent studies, by Corrigan (in press) and Vrolijk et al. (in press), of fission-track annealing in geologic settings have shown that Carlson's (1990) model does not accurately account for the low-temperature annealing behavior of tracks in apatite. The forward model of Crowley et al. (1991) best fits the data from the long-term geologic studies. The model of Carlson (1990) can be modified to fit the FT annealing data in the geologic settings mentioned above if an initial track length of 15.4 p.m is used. A comparison of predictions from the three published annealing models with the FT length data of Corrigan (in press) from south Texas is shown in Fig. 2. In addition, the modified model of Carlson (1990) predicts a mean track length of 14.9 µm for FT data from the East Marianna Basin, which is comparable to the mean length of 14.6 ± 0.1 p.m observed by Vrolijk et al. (in press).

In this study, the algorithm of Corrigan (1991) is used to estimate cooling curves for samples with more than 50 confined track-length measurements, with monocompositional apatite populations, and with ages passing the Chi-squared test. An initial track length of 15.4 p.m is used to empirically correct Carlson's equations so that the model fits the behavior of tracks in a geologic setting. The average rate of cooling for samples from each mountain block in the temperature range of 120 to 60°C, which is the temperature range best constrained by track-length analysis, is pre-

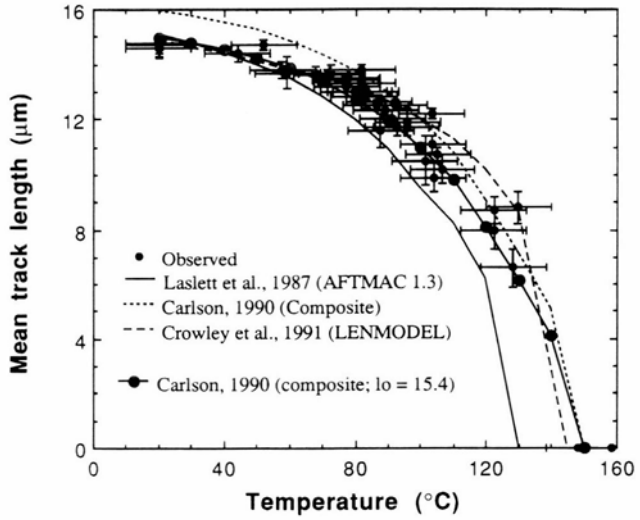

FIGURE 2—Observed mean track-length versus present temperature for south Texas data compared to mean track-length predicted by Laslett et al.'s (1987) preferred fanning model, Carlson's (1990) model, Crowley et al.'s (1991) model, and Carlson's (1990) model with a mean initial length of 15.4 µm.

sented in Table 1. Contour plots which show where 99, 95, 75, and 50% of the solutions that satisfy the data lie were used in evaluating changes in cooling rate through time; the 50 or 75% contours at the interior of the solution envelope delineate where the cooling history is best constrained. The cooling rate between 120 and 60°C is determined from the following simple relation:

$$\text{cooling rate} = 120°C - 60°C / t_{120} - t120$$

where t120 = the time at the center of 50 or 75% envelope at 120°C and t60 = the time at the center of 50 or 75% envelope at 60°C. The average cooling rate is independently calculated using a program that determines the gradient of each successful solution. Uncertainties in the cooling-rate estimates are on the order of ± 1 to 2°C/Ma for cooling rates of 1 to 5°C/Ma, and ± 3 to 4°C/Ma for cooling rates of 10 to 15°C/Ma. There is currently much debate concerning the quantitative models proposed to describe fission-track annealing (Crowley, in press; Corrigan, in press), and we thus consider the cooling rates presented here to be order-of-magnitude estimates. Furthermore, since the geothermal gradient is unlikely to have remained constant during rift development, denudation rates cannot be calculated directly from these cooling rates.

Results

The location of each traverse examined in this study is shown in Fig. 1. Microprobe data for apatite from selected samples from the flanks of the rift are summarized in Table 2. The microprobe results indicate that most of the apatite from rocks exposed in this area contains little chlorine. Only two sandstones from the Manzano Mountains, two sandstones from the Sierra Nacimiento, one sandstone from the Sangre de Cristo Mountains, and a gabbro from Blanca Peak contain apatite grains with chlorine contents greater than the apatite standard from Durango, Mexico. No correlation between individual-grain age and composition was observed in any of the samples.

The interpretation of the FT data for each traverse is considered in detail in the following sections; the areas are discussed in order from north to south. The cooling rates estimated from the FT results are shown in Table 1. Track-length histograms and cooling histories of representative samples are presented below; the complete set of FT data for all samples is available from the authors on request.

Sawatch Range

Twelve samples were collected from the 36.6 Ma Mt. Princeton Granite (Shannon, 1988), which is located in the Sawatch Range on the west side of the Upper Arkansas Basin near Buena Vista, Colorado. The Upper Arkansas Basin is a half-graben tilted to the west—southwest (Fig. 1). The Mt. Princeton batholith is believed to be the source for the 36.6 Ma Wall Mountain Tuff in the Thirtynine Mile volcanic field to the east of the rift (Shannon, 1988). Super-

TABLE 1—Cooling rates in the temperature range of 60 to 120°C estimated from inversion model. Time interval refers to the average time the samples have needed to pass through 60 and 120°C, respectively.

Mountain range	Sample	Time interval (Ma)	Cooling rate (°C/Ma)	Mountain range	Sample	Time interval (Ma)	Cooling rate (°C/Ma)
Sawatch	84MP02	7-11	15	Santa Fe	81SF03	25-42	4
	84MP03	5-11	10		81SF04	25-58	2
	84MP04	5-10	13		81SF05	21-55	2
	84MP05	4- 8	15		81SF06	23-72	1
	84MP06	11-17	10		81SF08	27-50	3
	84MP07	11-16	12		81SF10	35-55	3
	84MP08	12-18	10		81SF11	35-60	2
	84MP09	6-14	8		81SF14	22-83	1
	84MP10	12-19	9		81SF15	21-50	2
	84MP11	14-21	9				
	84MP12	11-18	9				
				Sandia	81SAN03	22–27	12
Sangre de	88SG03	4- 7	20		81SAN05	21–26	12
Cristo	88SG06	19-29	6		81SAN06	14–21	8
	88SG07	25-40	4		81SAN07	10–18	7
	88SG08	5-14	7		81SAN08	12–19	8
	88SG09	10-15	12		81SAN09	12–20	7
	88SG10	10-40	2		81SAN10	8–15	8
	88SG11	7-22	4		81SAN13	8–16	7
	88SG12	10-21	5		81SAN14	12–18	10
	88SG13	12-17	12		81SAN15	15–22	8
	88SG23	16-42	2				
				Manzano	88MAN03	10–28	3
Nacimiento	88NAC01	11-38	2		88MAN04	8–22	4
	88NAC02	16-36	3				
	88NAC05	25-53	2	Sierra	88LAD01	7–11	15
	88NAC06	20-75	1	Ladrones	88LAD02	9–12	20
	88NAC08	40-12	2		88LAD03	7–10	20
	88NAC09	15-65	1		88LAD04	7–10	20
	88NAC10	8-50	1		88LAD05	8–11	20
	88NAC11	8-33	2		88LAD06	7–12	12
	88NAC13	23-45	3				

imposed on the Mt. Princeton batholith is the 33.4 Ma Mt. Aetna caldera, which in turn is intruded by 29.8 Ma granites along the southeastern margin of the caldera (Shannon et al. 1987; Shannon, 1988). The Sawatch Range has been deeply eroded, obliterating the caldera source of the Wall Mountain Tuff and exposing structurally deep levels of the Mt. Aetna caldera. In contrast, the Mosquito Range on the east side of the Arkansas half-graben has not been as deeply eroded because the outflow sheets from the Mt. Princeton batholith and Mt. Aetna caldera are preserved (Shannon, 1988).

Geothermal activity extensively altered the Mt. Princeton batholith along the eastern margin of the Sawatch Range during the late Tertiary. Mt. Princeton Hot Spring, located along the western boundary fault of the Upper Arkansas

TABLE 2—Chlorine concentrations in Rio Grande rift apatite. For reference, Durango apatite contains 0.40 wt % chlorine. Five to twenty analyses were run for each sample.

Mountain range	Sample number	Rock type	Range in wt % chlorine
Sawatch	84MP02	Quartz monzonite	0.27–0.32
Sangre de Cristo	88SG01	Gneiss	0.00–0.27
	88SG03	Granite	0.02–0.09
	88SG05	Sandstone	0.04–0.09
	88SG06	Sandstone	0.10–0.46
	88SG07	Sandstone	0.05–0.10
	88SG08	Sandstone	0.11–0.35
	88SG09	Sandstone	0.03–0.20
	88SG10	Sandstone	0.03–0.22
	88SG11	Sandstone	0.03–0.20
	88SG12	Gneiss	0.02–0.09
	88SG13	Gabbro	0.23–0.51
	88SG14	Granite	0.02–0.07
	88SG16	Granite	0.05–0.13
	88SG23	Granite	0.00–0.31
Sierra Nacimiento	88NAC06	Sandstone	0.01–0.05
	88NAC08	Granite	0.08–0.14
	88NAC10	Sandstone	0.08–0.50
	88NAC11	Sandstone	0.00–0.19
	88NAC13	Sandstone	0.10–0.59
	88NAC15	Sandstone	0.13–0.39
	88NAC16	Granite	0.03–0.20
Sandia	81SAN05	Granite	0.00–0.02
Santa Fe Range	81SF03	Granite	0.00–0.07
	81SF13	Granite	0.00–0.03
Sierra Ladrones	88LAD01	Granite	0.04–0.06
	88LAD06	Granite	0.02–0.13
Lemitar	90LEM01	Granite	0.03–0.09
Magdalena	89MAG09	Gabbro	0.04–0.13
	89MAG11	Gabbro	0.02–0.18
	89MAG12	Gabbro	0.11–0.29
Manzano	88MAN01	Sandstone	0.08–0.71
	88MAN03	Granite	0.08–0.15
	88MAN04	Granite	0.09–0.14
	88MAN05	Schist	0.05–0.21
	88MAN11	Schist	0.02–0.06
	88MAN12	Schist	0.02–0.09
	88MAN13	Sandstone	0.20–0.86
	88MAN18	Sandstone	0.03–0.30
Los Pinos	88LP01	Metarhyolite	0.03–0.06
	88LP05	Granite	0.00–0.04
	88LP06	Granite	0.00–0.08
	88LP08	Gneiss	0.02–0.21

Basin, is the present-day manifestation of this geothermal activity. Sharp (1970) found leonardite, a calcium zeolite, in the altered area of the batholith; he estimated that the zeolite formed at temperatures of 195 to 220°C and at depths of 1500 to 2000 m below the surface. He concluded that about 1800 m of erosion has taken place since the middle Tertiary.

Apatite FT ages determined by Church and Bickford (1971), Cunningham et al. (1977), Olson et al. (1977), Bryant and Naeser (1980), and Shannon (1988) on Proterozoic and Paleocene rocks in the Sawatch Range indicate that the bulk of the mountain block away from the Arkansas half-graben was uplifted during the Eocene to Oligocene (45 to 30 Ma) concurrent with the development of a regional erosion surface. The apatite FT ages of Bryant and Naeser (1980) and Shannon et al. (1987) on the Paleocene Twin Lakes stock, located north of the Mt. Princeton area, indicate cooling of the western part of the block during uplift and erosion in the late Oligocene to middle Miocene (16 to 30 Ma). The general increase in apparent apatite FT age from east to west in the Sawatch Range has been interpreted to reflect westward rotation of the block during rift formation.

A horst block that formed during rift development along the eastern side of the Mt. Princeton pluton has been mapped by Shannon (1988) (Fig. 3). The 7 to 8 km wide Collegiate Peaks horst has been identified on the basis of structural discontinuities across the margins of the horst; the presence of abundant north-trending faults within the horst; and the resetting of apatite FT ages in the block. Shannon (1988) estimated 500 to 800 m of offset along the western margin of the horst.

The samples collected in this study show that a middle to late Miocene thermal event, presumably related to the hydrothermal alteration described by Sharp (1970), is superimposed on cooling due to uplift and erosion in the east-central Sawatch Range. Five samples (84MP01-84MP05, Fig. 3) were collected on the eastern face of the range just north of Mt. Princeton Hot Springs, within the zone of zeolite alteration. The apatite ages in this region vary from 9.5 ± 1.6 to 14.1 ± 3.6 Ma with mean track lengths of 12.9 to 13.5 p.m and standard deviations of 2.0 to 2.6 p.m. The apparent ages show good correlation with elevation (Fig. 4, closed squares). The track-length histogram for 84MP04 in Fig. 5 is representative of the track-length distributions found in the heavily altered portion of the batholith. The FT data record recent rapid cooling on the order of 9 to 15°C/Ma.

Seven samples (84MP06-84MP12, Fig. 3) were collected in the range away from the mountain front, although 84MP09-84MP12 are within a weakly altered, faulted, and fractured portion of the pluton. The samples in this altered area have more variable thermal histories compared to the samples from along the range front to the east and the high-elevation samples (84MP06-84MP08) to the west. The apatite ages in the zone of weak alteration are older (14.8 ± 1.9 to 20.1 ± 2.3 Ma) and the mean track lengths are generally longer (13.5 to 14.5 p.m with standard deviations of 1.6 to 2.6 p.m) than those determined along the mountain front. The cooling rates are generally on the order of 6 to 8 °C/Ma. An example of the type of cooling history observed in this group of samples is shown in Fig. 5 (84MP10). In contrast to the interpretation of Shannon (1988), the minor relative uplift on the west side of the Collegiate Peaks horst does not seem to have a major effect on the FT ages, given the similarity in the ages and thermal histories of 84MP12 which lies on the horst, and 84MP11 which is to the west of the horst (Tables 1, 3). Instead, the variable thermal histories recorded by the four FT samples from this part of the batholith seem to be controlled more by hydrothermal fluids moving through fractures in the granite.

The samples at high elevation (84MP06-84MP08) have nearly identical histories, with apatite FT ages of 22.9 ± 5.0 Ma to 23.1 ± 5.6 Ma and mean track lengths of 14.5 ± 1.6 p.m. These samples cooled in two stages: (1) 25 to 8 Ma at a rate of about 7 to 10°C/Ma, and (2) 8 to 0 Ma at a rate of 3 to 4°C/Ma (Fig. 5, 84MP06).

In summary, elevated geothermal gradients associated with a middle to late Miocene hydrothermal system along

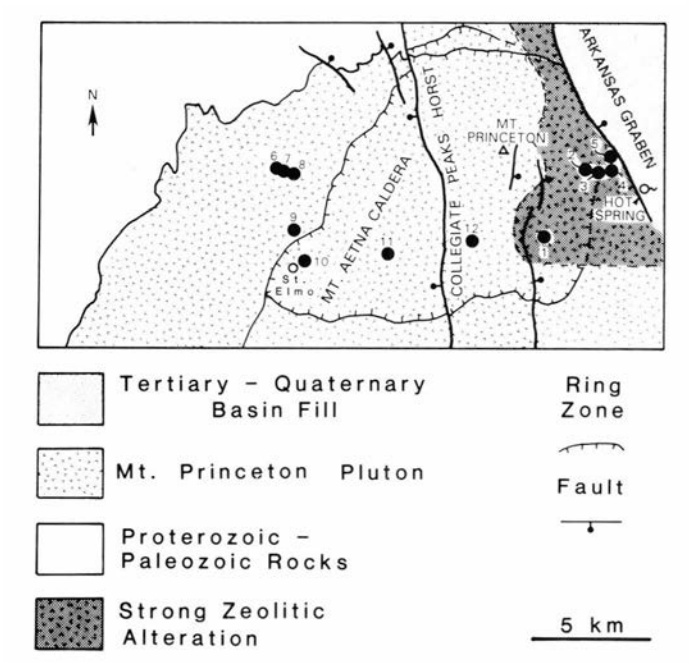

FIGURE 3—Generalized geologic map and sample localities for Mt. Princeton batholith, Sawatch Range, Colorado. Geology after Shannon (1988) and location of zeolite-alteration zone from Olson and Dellechaie (1976). Sample numbers are shown on the map, FT data for the samples are in Table 3.

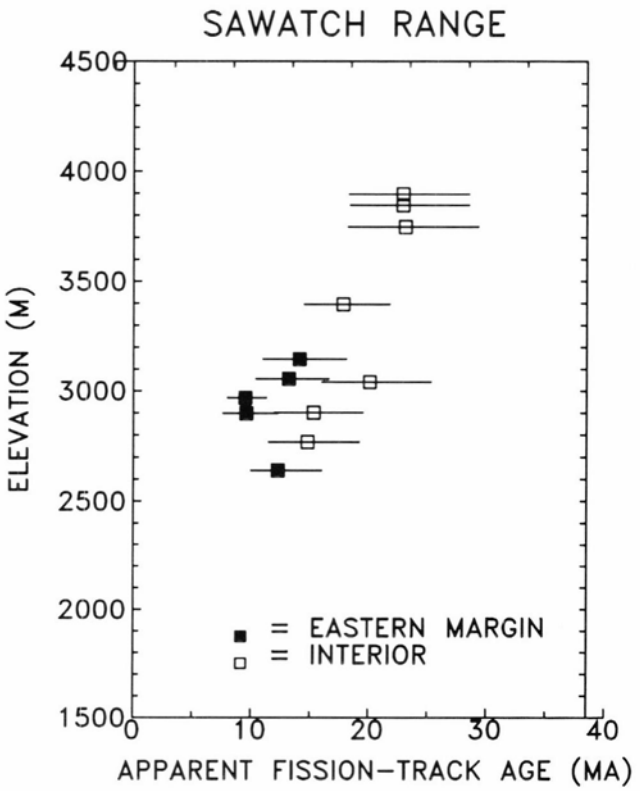

FIGURE 4—Age versus elevation plot for Mt. Princeton batholith samples.

the range front kept the east side of the pluton at high temperatures until denudation associated with late rift formation caused rapid cooling. The high-elevation portion of the pluton well to the west of the range front cooled relatively rapidly, primarily during the early phase of rift formation. The four samples collected between the range-front and the high-elevation samples have been affected by both early rift denudation and by the hydrothermal system. In the Mt. Princeton portion of the Sawatch Range, the general increase in apatite FT age to the west is more likely controlled by the presence of a fossil geothermal system than by rotation of the block to the west, although moderate tilting cannot be ruled out.

Sangre **de Cristo Mountains**

The Sangre de Cristo Mountains in Colorado are a long, narrow uplift composed primarily of Proterozoic metamorphic and igneous rocks and Paleozoic sedimentary rocks with minor Tertiary intrusives. Tweto (1979) noted that the Sangre de Cristo Mountains in this region are made up of two segments that join in the vicinity of Blanca Peak, where the range is cut by numerous transverse faults (Fig. 6). The north—northwest-trending northern segment is bound on both sides by Neogene faults. The Sangre de Cristo fault along the western side of this segment has been active during the Holocene (Knepper, 1976), while the Alvarado fault on the eastern side has had no Quaternary movement (Tweto, 1979). The north-trending southern segment (Culebra Range) is bound on the west by a complex zone of Neogene and Quaternary faults (Tweto, 1979). Some of the Quaternary faults have been active during the Holocene. Faults on the east side of the southern segment were active during the Laramide orogenic event (Cretaceous to Eocene) and possibly during the Neogene. No Quaternary movement has been identified along the eastern margin of the range. FT data from this area are of interest because little is known about details of the timing of the early phase of rift deformation in the two segments of the Sangre de Cristo Mountains.

Brister and Cries (in press) determined the general Cenozoic history of the region through analysis of seismic and well data from the San Luis Basin. Eocene sediments in the western part of the basin indicate that portions of the San Luis Basin were sites of deposition during the late stages

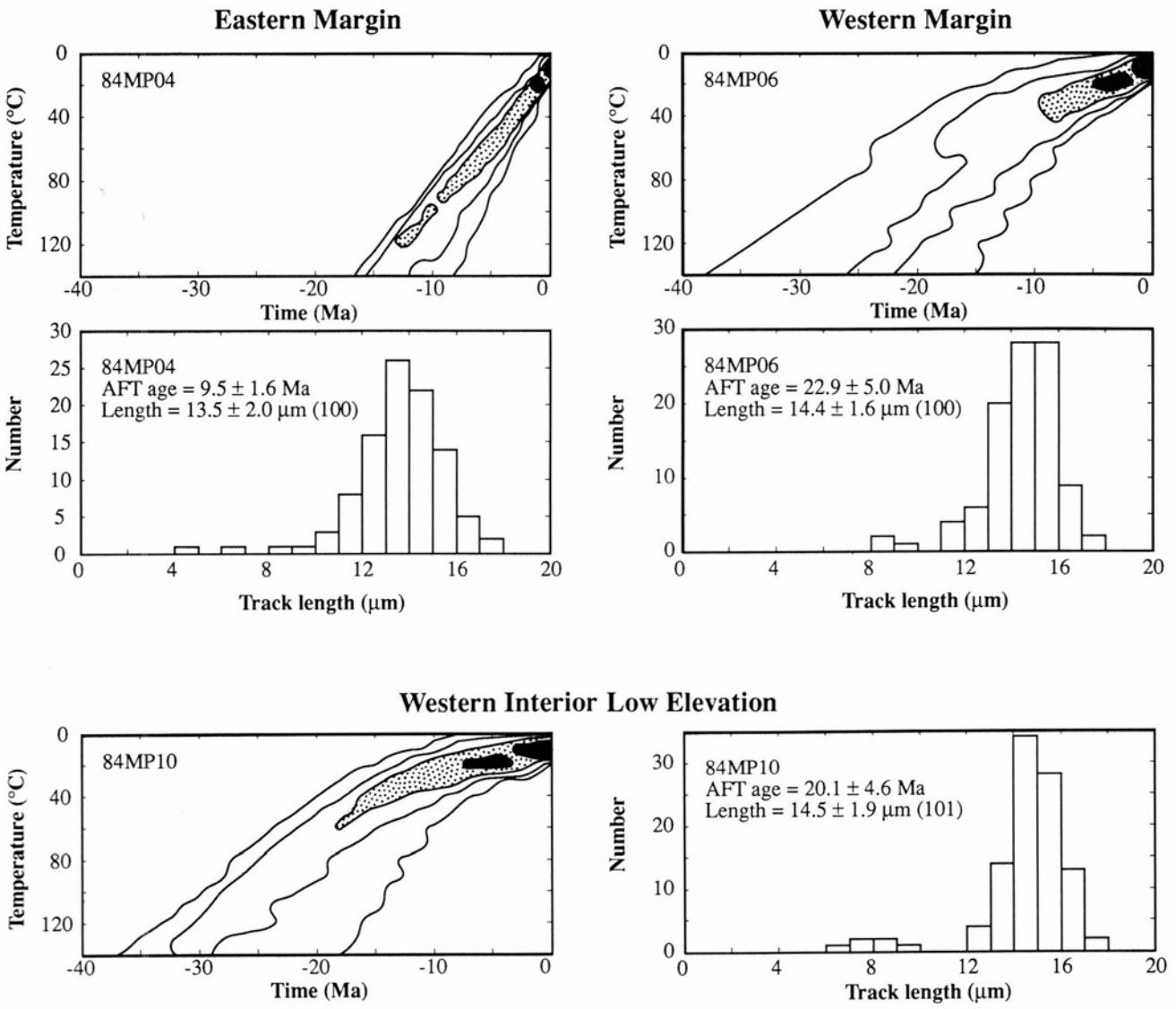

FIGURE 5—Representative track-length distributions and thermal histories for samples from the Mt. Princeton batholith. See Fig. 3 for locations. Contour plots are used to depict the thermal history. 50% of the solutions lie in the shaded region, 75% lie in the stippled region, and the outer envelopes enclose 90 to 99% of the solutions, respectively. The number in parentheses following the track-length measurement corresponds to the number of confined tracks measured.

TABLE 3—Apatite fission-track ages for Sawatch Range, Colorado. Zeta = 351 ± 40.

Sample number	Grains counted	Fossil tracks Tracks/cm² (x10⁵)	Fossil tracks #Tracks counted	Induced tracks Tracks/cm² (x10⁶)	Induced tracks #Tracks counted	Age (standard error) (Ma)	95% Confidence limits (Ma)	CHI² (%)	Uranium content (ppm)	Mean track length (s.e.) (μm)	N
84MP01	20	0.75	80	4.14	2196	12.3 (1.5)	16 10	97	36	13.3 (1.2)	14
84MP02	20	1.00	80	1.56	1249	14.1 (1.8)	18 11	99	21	13.5 (0.5)	101
84MP03	20	0.92	94	1.55	1593	13.2 (1.5)	17 10	99	21	13.5 (0.4)	100
84MP04	20	1.97	193	4.69	4598	9.5 (0.8)	11 8	75	60	13.5 (0.4)	100
84MP05	20	0.70	83	1.66	1974	9.6 (1.2)	12 8	55	21	12.9 (0.5)	100
84MP06	20	1.69	112	1.72	1139	22.9 (2.5)	28 18	75	21	14.3 (0.3)	100
84MP07	20	1.51	114	1.55	1174	22.9 (2.5)	28 18	97	18	14.6 (0.3)	100
84MP08	20	1.50	92	1.55	951	23.1 (2.8)	29 18	85	18	14.5 (0.3)	100
84MP09	20	1.46	138	1.99	1880	17.8 (1.8)	22 14	97	24	13.5 (0.5)	100
84MP10	20	1.61	98	1.96	1196	20.1 (2.3)	25 16	98	24	14.5 (0.4)	101
84MP11	20	1.15	86	1.87	1397	15.3 (1.9)	20 12	95	21	14.5 (0.5)	100
84MP12	20	1.07	74	1.82	1256	14.8 (1.9)	19 12	99	21	14.2 (0.4)	100

of the Laramide event. Beveling of the region occurred in the late Eocene. Volcanic rocks, primarily from the San Juan volcanic field, then covered the beveled surface in the Oligocene. The San Luis Basin formed as a broad half-graben tilted to the east; it was filled with sediments of the latest Oligocene to Pleistocene Santa Fe Group derived from the rising Sangre de Cristo and San Juan Mountains.

Lindsey et al. (1986) used the distribution of low-grade metamorphic rocks, altered conodonts, and apatite FT ages from Pennsylvanian-Permian sedimentary rocks and Precambrian gneissic rocks located in the northern segment of the Sangre de Cristo Mountains near Creston (Fig. 6, profile A) to infer the thermal history of this portion of the range. Rocks in this part of the range were heated by burial beneath late Paleozoic and Mesozoic sedimentary rocks, by burial during Laramide thrusting and folding, and locally by Oligocene volcanic and intrusive activity. The heating events discussed by Lindsey et al. (1986) for the area around profile A in Fig. 6 likely affected the Sangre de Cristo Mountains as a whole, although the relative importance of each of the heating mechanisms varies along the range. The area studied by Lindsey et al. (1986) subsequently cooled at approximately 19 Ma during early rift development (apatite FT ages of 15 to 24 Ma). Although no track-length analyses were presented by Lindsey et al. (1986), they concluded that the uplift of this part of the range must have been rapid since the age is weakly correlated with elevation.

The samples dated by Lindsey et al. (1986) were kindly provided to us, and we were able to obtain statistically meaningful track-length distributions for two of the samples, 221 and 222. The length distributions are unimodal and skewed toward long tracks; mean track lengths for the samples are 14.5 ± 1.5 μm and 14.2 ± 2.5 μm, respectively. Less than 40 confined tracks were found in each sample, so no detailed modeling of the cooling history was attempted. Cooling rates of approximately 6 to 9°C/Ma can be inferred from the track-length data; these rates are consistent with the conclusions of Lindsey et al. (1986).

The FT samples for this study (Table 4) were collected along five traverses between the profile of Lindsey et al. (1986) and the profile of Kelley and Duncan (1986) in the Taos Range portion of the Sangre de Cristo Mountains (Fig. 6). The five traverses are (from north to south) Mosca Pass, Blanca Peak, La Veta Pass, Trinchera Peak, and Culebra Peak.

Mosca Pass—Three datable samples were collected from Proterozoic granitic and gneissic rocks and from the strongly deformed and metamorphosed Pennsylvanian Minturn Formation at Mosca Pass. The FT results from this area are interesting in that they are among the youngest FT ages determined in this study, ranging from 6 ± 1 Ma at low elevation to 13 ± 2 Ma at high elevation (Fig. 7). Well constrained track-length data are available for only 88SG03, which has a mean track length of 14.0 ± 2.0 p.m. The cooling rate for this sample is approximately 20°C/Ma (Fig. 8).

This portion of the range lies within the transition zone between the northern and southern segments of the Sangre de Cristo Mountains. To the east of the traverse, the transition zone is bisected by a narrow, north-trending graben containing 30 to 35 Ma andesites and Miocene sedimentary rocks (Tweto, 1979). The reasons for the young FT ages from this profile are not known, but they may be related to intrusions or to high heat flow associated with the complex structures in this transition zone.

Blanca Peak—The apatite FT ages on Proterozoic crystalline rocks exposed on the southwest side of Blanca Peak (Fig. 6; SG13, 14, 16) vary from 18 ± 4 Ma on the summit to 16 ± 10 Ma at lower elevations (Fig. 7). The ages and track-length distributions for the low-elevation samples are

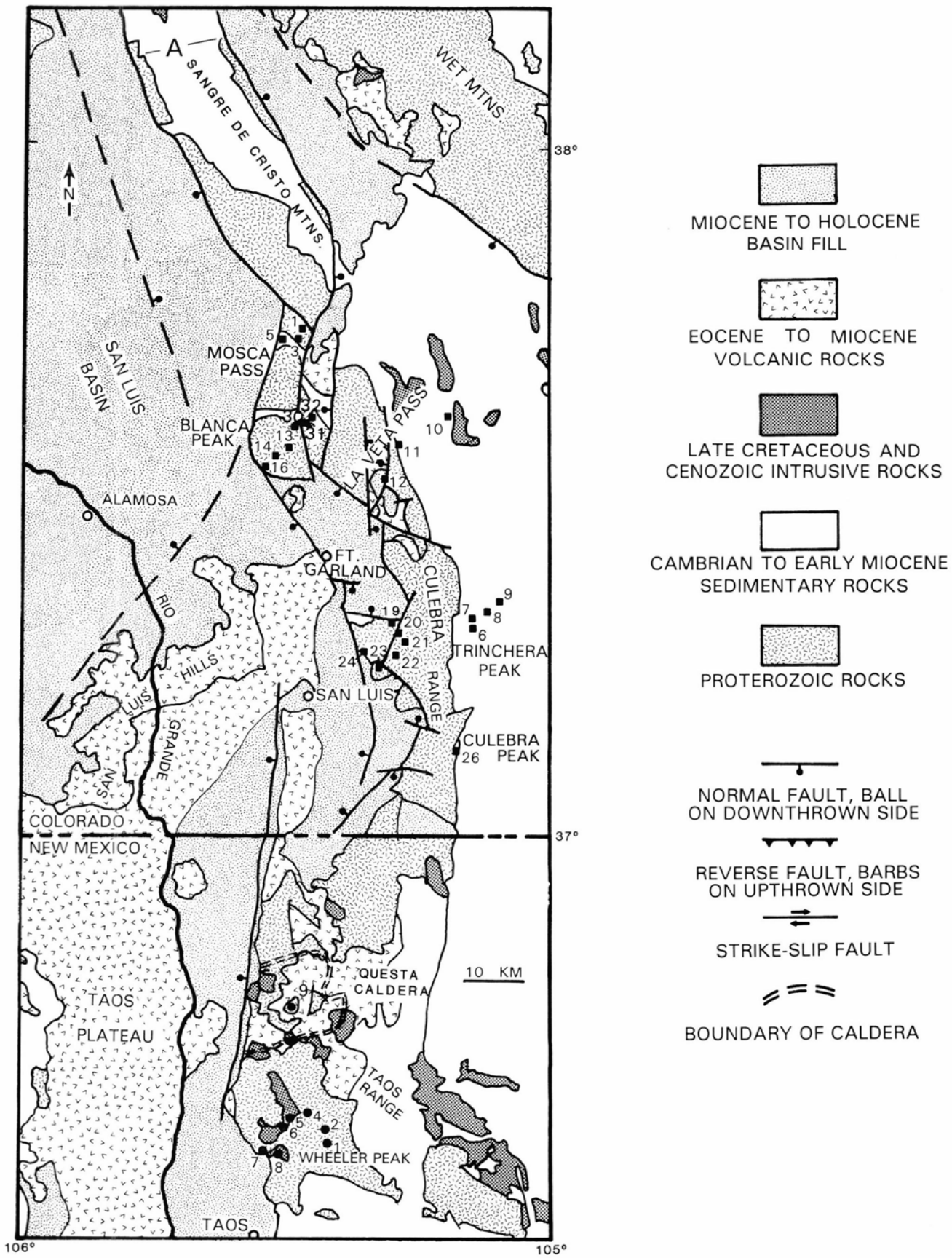

FIGURE 6—Generalized geologic map and sample localities in the Sangre de Cristo Mountains. Geology after Tweto (1978) and Woodward et al. (1978). Sample numbers are shown on the map, FT data for samples are in Table 4. The profile of Lindsey et al. (1986) is labeled as A. Samples in the Taos Range from Kelley and Duncan (1986) are shown as circles numbered 1–8 in southern part of the map.

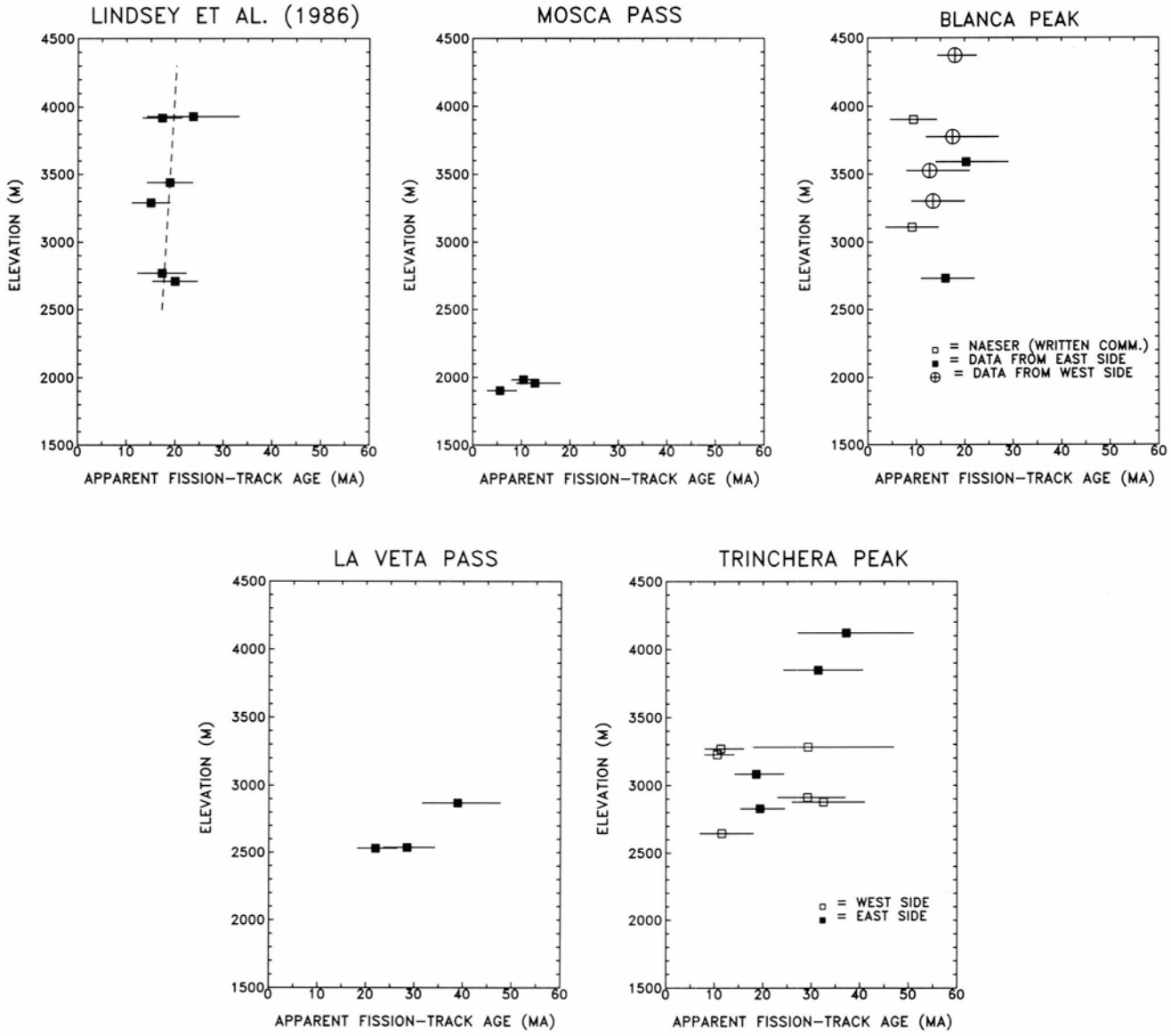

FIGURE 7—Age versus elevation plots for Sangre de Cristo Mountains.

not well constrained due to low uranium concentrations in these apatites, which results in low track counts. The FT ages presented in this paper for 88SG14 and 88SG16 are different from those published by Kelley (1990) because the samples were re-evaluated. In an attempt to more tightly constrain the age of these low-uranium samples, 40 instead of the usual 20 grains were counted. As a consequence, much of the age scatter as a function of elevation was removed. The more tightly constrained ages are within the error of ages independently determined by Naeser (written comm. 1991) for this area.

FT ages from the northeast side of Blanca Peak (90SG30-90SG32) are similar to those from the southwest side. The highest-elevation sample at Lilly Lake has an age of 17.5 ± 3.7 Ma, and the low-elevation samples have ages of approximately 13 Ma. Modeling of the track-length data from the summit (88SG13, Fig. 8) and the lack of correlation of age with elevation over such a large elevation change (Fig. 7) indicate that this portion of the Sangre de Cristo Mountains experienced rapid cooling (≈12°C/Ma) between 20 and 12 Ma.

La Veta Pass—Samples from La Veta Pass (Fig. 7, 88SG10-88SG12) yield FT ages of 39 ± 8 Ma for the Pennsylvanian-Permian Sangre de Cristo Formation at high elevation, 28 ± 5 Ma for the Pennsylvanian Minturn Formation at lower elevation, and 22 ± 4 Ma for a Proterozoic gneiss low on the west side of the pass (Fig. 7). The mean track lengths for these samples increase from 12.4 ± 2.3 to 13.2 ± 2.8 μn with decreasing elevation.

The FT data for the high-elevation sample, 88SG10 (Fig. 8), indicate that this sample cooled slowly (2°C/Ma), spending a significant amount of time in the zone of partial stability for apatite. This sample was probably brought near the surface during Laramide deformation and subsequent Eocene erosion. This high-elevation portion of the Sangre de Cristo Mountains remained at a relatively shallow level in the crust (2 to 3 km) until it was brought to the surface during rift development. The low-elevation Proterozoic gneiss, 88SG12 (Fig. 8), cooled relatively rapidly (5°C/Ma) as a consequence of denudation and waning volcanism during early rift formation.

Trinchera Peak—The only complete traverse through the range starts on the east near Spanish Peaks, passes through Trinchera Peak, and terminates on the western margin of a complexly faulted block of Proterozoic granite that projects into the San Luis Basin northeast of the village of San Luis.

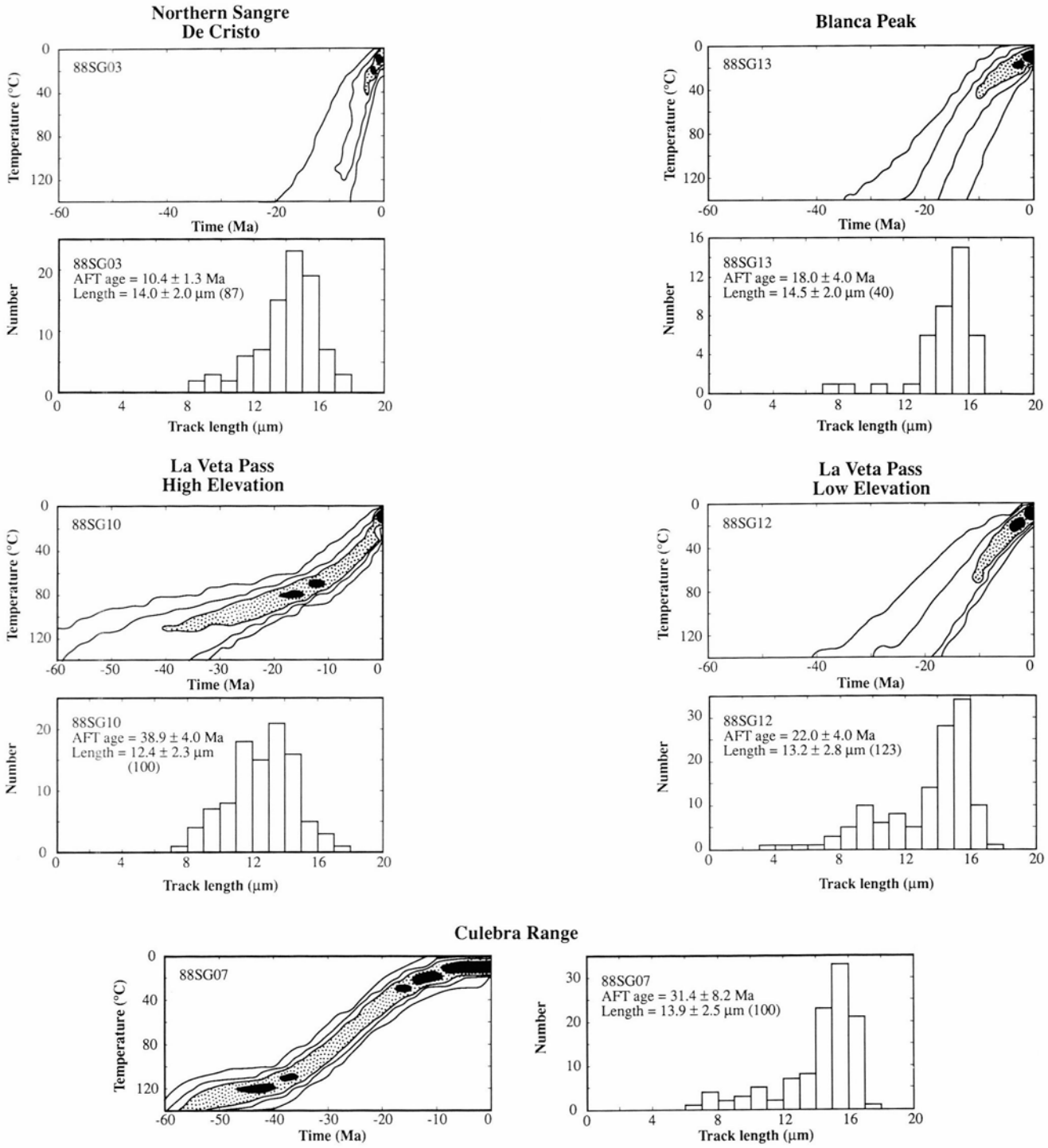

FIGURE 8—Representative track-length distributions and thermal histories for samples from the Sangre de Cristo Mountains. See Fig. 6 for locations.

Sandstones from the Pennsylvanian to Permian Sangre de Cristo and Minturn Formations exposed on the east side of the range in the vicinity of Trinchera Peak (Fig. 6, 88SG06—88SG-09) have ages of 37 ± 6 Ma at high elevations, decreasing to 19 ± 2 Ma at low elevations near the Spanish Peaks intrusive complex (Fig. 7). Mean track lengths for the samples range from 13.1 to 14.1 p.m. The highest samples (88SG06 and 07, Fig. 8) cooled slowly (4 to 6°C/Ma) compared to the low-elevation samples near Spanish Peaks (7 to 12°C/Ma, 88SG08 and 09). Like the high-elevation sample from La Veta Pass, samples from high on Trinchera Peak have a history largely controlled by cooling as the result of Eocene erosion. Data from the low-elevation samples on the east side of the range reflect cooling following the Spanish Peaks intrusive event (20 to 25 Ma; Smith, 1979).

The cooling history of the western margin of the Culebra Range is very complex. The apparent FT ages along the west side vary between 10 ± 2 to 32 ± 4 Ma and show no correlation with elevation. The youngest ages (10 to 11 Ma) are generally located along the axis of a promontory that extends into the San Luis Basin. Gold mining activity on the western edge of the promontory (Jones and Benson, 1990) suggests the possibility that hydrothermal fluids associated with mineralization may have altered the FT ages.

TABLE 4—Apatite fission-track ages for Sangre de Cristo Mountains, Colorado. Zeta = 351 ± 40.

Sample number	Grains counted	Fossil tracks Tracks/cm² (x10⁵)	Fossil tracks #Tracks counted	Induced tracks Tracks/cm² (x10⁶)	Induced tracks #Tracks counted	Age (standard error) (Ma)	95% Confidence limits (Ma)	CHI² (%)	Uranium content (ppm)	Mean track length (s.e.) (μm)	N
88SG01	20	0.25	34	1.52	1031	12.8 (2.3)	18 9	99	12	13.0 (1.2)	14
88SG03	20	0.49	73	3.67	2716	10.4 (1.3)	13 8	95	27	14.0 (2.0)	87
88SG05	20	0.18	17	2.49	1170	5.6 (1.4)	9 3	99	18	-	-
88SG06	16	1.02	55	1.00	267	37.2 (5.9)	51 27	95	15	13.7 (0.6)	73
88SG07	20	1.12	86	1.28	490	31.4 (4.1)	41 24	99	21	13.9 (0.5)	100
88SG08	20	1.34	74	2.56	705	18.6 (2.5)	24 14	60	42	13.6 (0.4)	50
88SG09	20	0.85	106	1.54	961	19.4 (2.3)	24 15	25	24	14.5 (0.5)	83
88SG10	20	2.67	163	2.38	728	38.9 (4.0)	48 32	20	42	12.4 (0.4)	100
88SG11	20	2.50	220	3.02	1327	28.5 (2.6)	34 24	50	48	12.9 (0.4)	101
88SGI2	20	1.56	211	2.42	1634	22.0 (2.0)	26 18	25	42	13.2 (0.5)	128
88SG13	20	1.00	117	1.88	1096	18.0 (2.0)	22 14	99	30	14.5 (0.6)	40
88SG14	40	0.28	40	0.46	328	20.3 (3.5)	29 14	99	9	-	-
88SG16	40	0.22	42	0.44	424	16.0 (2.7)	22 11	99	9	-	-
89SG19	20	0.87	78	2.30	1033	29.3 (3.7)	38 23	97	18	15.0 (1.1)	6
89SG20	20	0.14	19	0.36	238	29.3 (7.1)	47 18	99	3	14.0 (1.2)	10
89SG21	20	0.27	39	1.82	1308	11.3 (1.9)	16 8	99	15	14.5 (0.9)	15
89SG22	17	0.55	53	4.03	1934	10.6 (1.5)	14 8	99	30	14.7 (0.5)	12
89SG23	20	0.59	87	1.40	1038	32.5 (3.9)	41 26	99	12	13.3 (0.3)	100
89SG24	18	0.17	19	1.18	639	11.5 (2.7)	18 7	99	9	-	-
89SG26	20	0.34	35	0.57	296	42.3 (7.9)	61 29	99	3	13.0 (0.9)	17
90SG30	20	0.23	26	1.94	1104	13.4 (2.7)	20 9	90	9	-	-
90SG31	20	0.32	24	1.94	737	17.5 (3.7)	28 12	99	9	-	-
90SG32	20	0.24	18	1.91	763	12.7 (3.1)	21 8	99	9	-	

Jones and Benson (1990) reported a 24 Ma K/Ar age for sericite alteration of rhyolite dikes at the El Plomo gold mine, and they also mentioned the presence of undated, post-mineralization andesite dikes in this area. Jones and Benson (1990) inferred that the mineralization at the El Plomo mine occurred at the same time as the sericitic alteration of the rhyolite dikes at 24 Ma, and that the location of the mineralization is controlled by a low-angle normal fault zone that formed prior to mineralization. Sample 89SG24 is from the brecciated fault zone at the El Plomo mine; the FT age data imply that the fault zone remained at elevated temperatures until approximately 10 Ma. The 10 to 11 Ma FT ages for 89SG21 and 89SG22 seem to indicate that the thermal anomaly associated with the mineralization may extend 5 to 10 km to the east of the mine.

Only one sample from the west side of the range (89SG23, Fig. 6) contained abundant confined tracks. Sample 89SG23 is located away from the gold mineralization, on the west side of a major down-to-the-west normal fault, and its cooling history (2°C/Ma) is similar to thermal history of rocks at high elevation that cooled during Eocene erosion. The presence of ages of approximately 30 Ma at low elevation on the west side of the Culebra Range suggests that this portion of the Sangre de Cristo Mountains may have been down-dropped during rifting.

One sample collected during this study on the Forbes

Ranch along the western margin of the Sangre de Cristo Mountains (89SG19) is a slightly reworked tuff that yields an apatite FT age of 29.2 ± 7.0 Ma. This tuff may correlate with the Ra Jadero Member of the Treasure Mountain Tuff in the San Juan Mountains (K/Ar age of 28.2 to 29.8 Ma; Lipman, 1975). Kearney (1983) found a similar tuff at La Veta Pass.

Culebra Peak—One sample, 89SG26, was obtained from Proterozoic gneiss on Culebra Peak. The FT age of 42 ± 15 Ma indicates that rocks at high elevation in this area were brought near the surface during Laramide deformation and Eocene erosion. Only 17 confined tracks, with a mean length of 13.0 ± 0.9 1.1µm, were observed in this sample, so detailed modeling was not possible. Proterozoic granites at lower elevation contain abundant fluorite and insufficient apatite for dating purposes.

Summary—The Sangre de Cristo Mountains north of La Veta Pass (near Blanca Peak), Colorado, cooled rapidly during the late Oligocene to late Miocene. The northern Sangre de Cristo Mountains are a narrow horst (≈18 km wide) between major normal faults that dip in opposite directions (Fig. 6). The deepest sides of the bordering half-grabens (San Luis Basin on the west; Wet Mountain Valley on the east) abut the range. Thus the range has a triangular cross-section and it experienced rapid istostatic uplift early in rift development. Similarly, Blanca Peak is bounded on three sides by faults, which allowed this pyramidal block to rise rapidly in the early to middle Miocene. In contrast, the La Veta Pass, Trinchera Peak, and Culebra Peak areas to the south record slow denudation in the Eocene, perhaps related to the development of the late Eocene erosion surface (Epis and Chapin, 1975), with cooling continuing into the early Miocene. The Culebra Range is a broad, east-tilted fault block with major normal faults on the west side. This portion of the range has denuded more slowly, allowing older ages to be preserved at higher elevation.

The northern Sangre de Cristo Mountains did not have high relief in the Oligocene. East-trending paleovalleys filled with volcanic rocks (Gribbles Park Tuff) of western provenance that are as young as 33 Ma (W. C. McIntosh, unpubl. 40Ar/39Ar ages) are preserved on the east side of the range at several localities (Epis et al., 1975). The presence of these paleovalleys indicates that the Sangre de Cristo Mountains did not exist as a topographic barrier at this time. The FT data are consistent with this geologic evidence. The southern segment of the Sangre de Cristo Mountains may also have had low relief (Tweto, 1979).

Oligocene to middle Miocene volcanism in southern Colorado locally affected portions of the northern Sangre de Cristo Mountains (Lipman, 1981; Steven, 1975). Consequently, the Miocene cooling recorded by the FT data is probably related to both denudation and relaxation of isotherms following the end of regional volcanism.

Northern New Mexico

Sierra Nacimiento—The Nacimiento uplift in northern New Mexico (Fig. 9) is a north-trending, east-tilted block of Proterozoic to early Cenozoic rocks bounded on the west by the oblique-slip Nacimiento fault zone (Baltz, 1967; Woodward, 1987). FT ages from Proterozoic granites and Paleozoic to Mesozoic sandstones exposed in the Sierra Nacimiento and its northern culmination, San Pedro Moun-

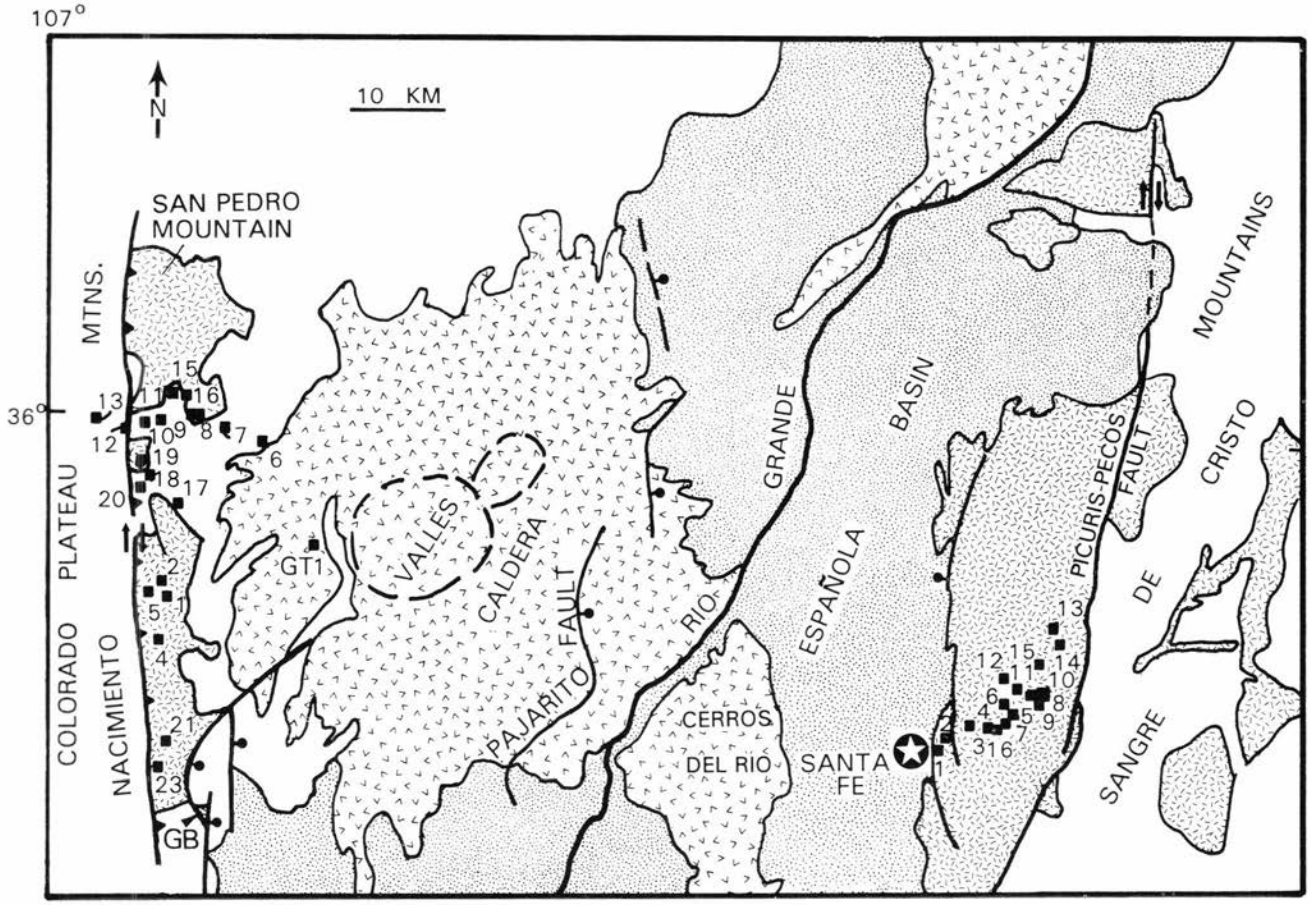

FIGURE 9—Generalized geologic map and sample localities in the Sierra Nacimiento and Santa Fe Range. Geology after Woodward et al. (1978). Sample numbers are shown on the map, FT data for samples are in Table 5. Samples in the Santa Fe Range from Kelley and Duncan (1986) are shown as 1–13 in eastern part of the map. GB = Guadalupe Box. GT-1, the Hot Dry Rock drill hole site for which Brookins et al. (1977) have FT data as a function of depth, is shown for reference.

tain, were determined in order to examine the evolution of an uplift along the western margin of the rift. Sedimentological evidence suggests that relief developed in this region during at least two phases of Laramide deformation in the Late Cretaceous to Paleocene and in the late Eocene to Oligocene (Baltz, 1967; Smith, 1991). Since the Oligocene to early Miocene Abiquiu Formation in the northeastern part of the block dips to the east, Baltz (1967) suggested that the block was tilted eastward during the Miocene to Pliocene.

Generally, the cooling rates for all samples from the Nacimiento uplift are quite low (1 to 3°C/Ma). The FT data demonstrate that the western portion of the Nacimiento uplift is made up of at least two blocks with slightly different cooling histories. The southern portion, the Sierra Nacimiento (Fig. 10, open squares) cooled during the middle Eocene to earliest Oligocene (46 ± 5 to 33 ± 4 Ma; mean lengths 13.0 to 13.8 ± 1.4-1.9 p.m), while the northern part, corresponding roughly with San Pedro Mountain (Fig. 10, solid squares), cooled between Late Cretaceous and middle Eocene (81 ± 8 to 46 ± 7 Ma; mean lengths 11.0 to 13.4 ± 1.6 to 2.4 p.m). Samples collected along a traverse between the northern and southern blocks have an intermediate age range (38 ± 6 to 56 ± 7 Ma). Figs. 10 and 11 show the slight difference in the cooling histories of the northern and southern blocks.

A component of difference in cooling history in the two blocks is related to the Late Cretaceous paleogeography of the region. During the Late Cretaceous, the northern portion of the Nacimiento uplift was a shoal, based on the lithology of, and unconformities in, the Cretaceous section preserved in the San Juan Basin to the west of the uplift (Baltz, 1967). The apatite in some of the Paleozoic rocks that rest on the Proterozoic granites in this block may never have been completely reset. For example, the individual grain ages for 88NAC15, a sample of the Permian Abo Formation that sits at high elevation on San Pedro Mountain, fail the Chi-square test, which indicates that multiple-age popula

tions are present. The chlorine content of the apatite does not seem to have been a factor (Table 2), so the scatter may be related to provenance. Since each source region contributing apatite to the Abo Formation may have had a unique thermal history, the present-day grain-age populations are probably a reflection of the original grain-age populations of the sandstone.

Differential uplift has also contributed to the difference in cooling history between the north and south blocks. Differential uplift of the block is supported by examination of structures in the Nacimiento uplift. Vertical displacement on the western border faults increases from south to north (Baltz, 1967), implying that the northern part of the block might have cooled before the southern part during Laramide deformation. In addition, several east-trending faults between the two sections (Woodward, 1987) apparently have accommodated some of the differential uplift. However, based on the FT results from the traverse between the northern and southern blocks, the differential uplift from south to north appears to be gradational, suggesting that the east-trending faults have small displacements.

Rotation of the block to the east is supported by the FT data. The 81 Ma date from the Abo Formation exposed along the eastern margin of the uplift (88NAC06; Fig. 9) indicates that this unit apparently was not buried as deeply nor as strongly uplifted as samples to the west. Similarly, an apatite fission-track age on a Precambrian sample at Guadaloupe Box (GB, Fig. 9) on the eastern side of the mountains yields an age of 251 ± 25 Ma (Brookins et al., 1977), which indicates that the eastern margin of the block was not significantly buried since the Permian nor strongly elevated during early Cenozoic deformation.

One sample of sandstone (88NAC13, Eocene San Jose Formation) was collected from the Colorado Plateau adjacent to the Nacimiento uplift (Fig. 9). The individual-grain ages for this sample failed the Chi-square test and the apatite compositions ranged from fluorapatite to chlorapatite

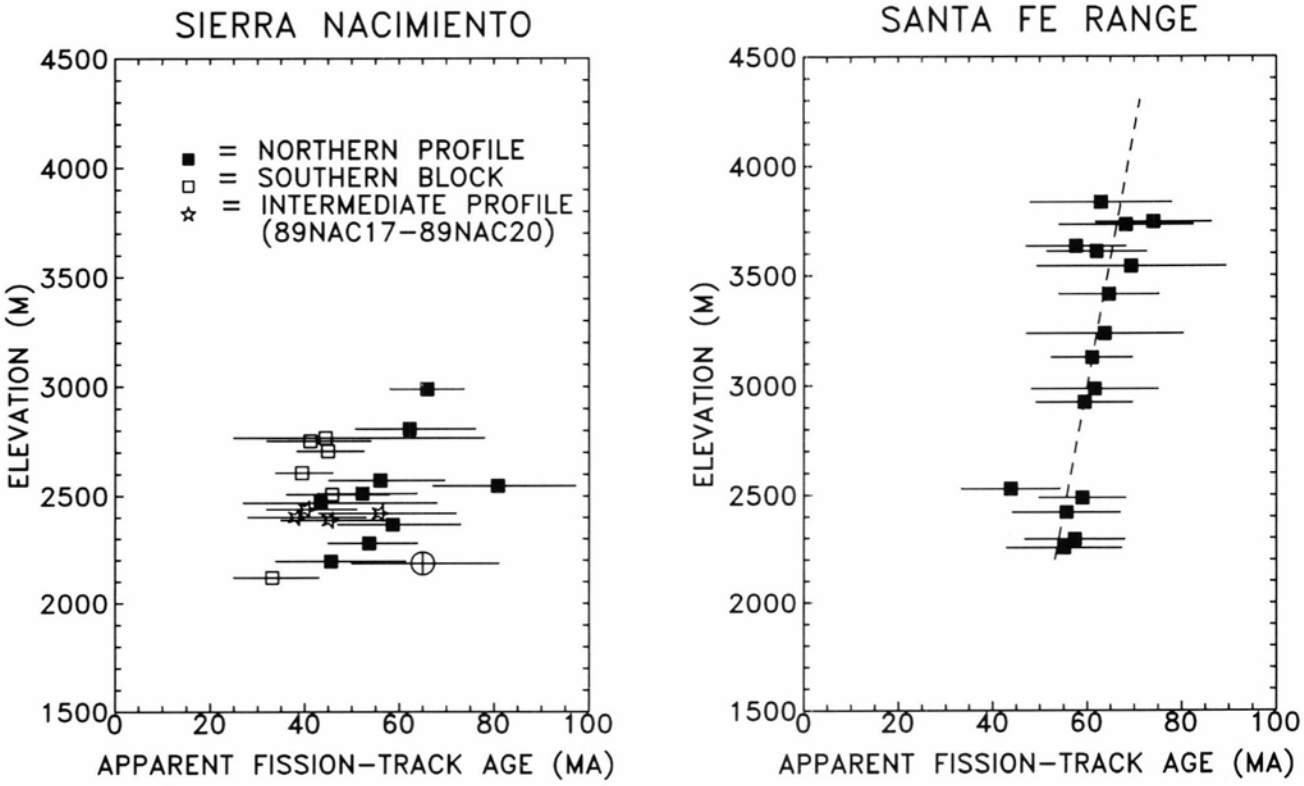

FIGURE 10—Age versus elevation plots for Sierra Nacimiento and Santa Fe Range.

(Table 1), implying diverse provenance for this sandstone. The mean track-length data (Table 5) and the fact that the FT age is older than the stratigraphic age indicate that this sandstone has not been significantly buried since deposition.

Santa Fe Range—FT data from the Santa Fe Range are discussed by Kelley and Duncan (1986) and Kelley (1990), and are summarized in Table 6. These data are briefly discussed here because the apatite FT ages from this area are anomalously old compared to other FT data from the rift.

The Santa Fe Range (Fig. 9) consists primarily of Proterozoic granitic and gneissic rocks bounded on the east by the Picuris–Pecos fault and on the west by an ill-defined fault zone in the Espanola Basin. The apatite FT ages from this mountain block are generally between 50 to 70 Ma (Fig. 10), and the track-length histograms are characteristic of samples that cooled slowly (1 to 3 °C/Ma; Fig. 11). Since the older FT ages are preserved, this area was not the site of significant denudation or deposition during late Laramide or early rift deformation. This mountain range is similar to portions of the Sierra Nacimiento in this regard.

Basin-fill sediments were probably deposited over the Santa Fe Range during early rift development. The range near Santa Fe may have formed the basement under the eastern portion of a broad, shallow, early Miocene Espanola Basin. The Tesuque Formation above the basal volcaniclastic

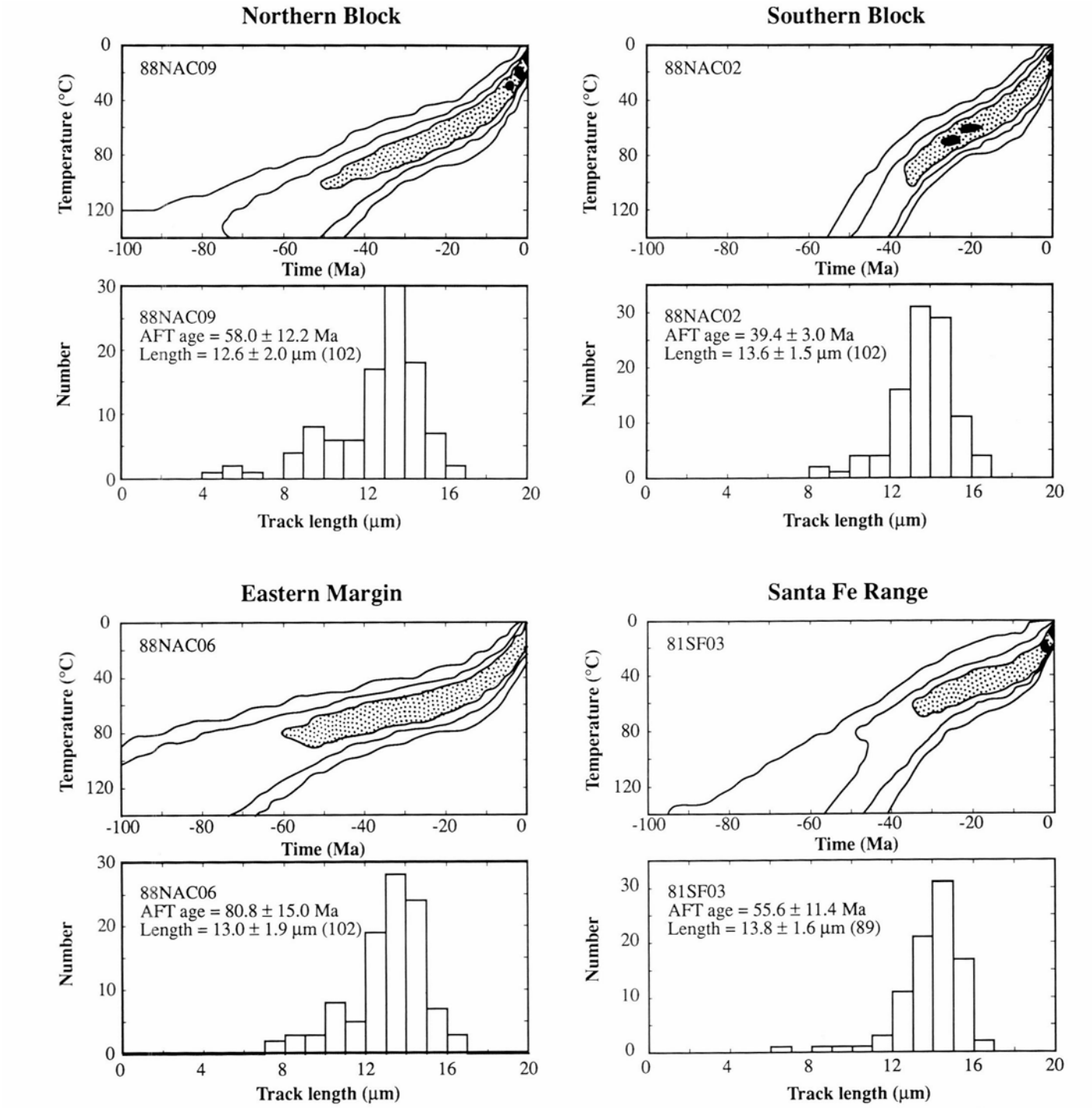

FIGURE 11—Representative track-length distributions and thermal histories for samples from the Sierra Nacimiento. A representative sample from the Santa Fe Range (Kelley, 1990) is shown for comparison. See Fig. 9 for locations.

TABLE 5—Apatite fission-track ages for Sierra Nacimiento, New Mexico. Zeta = 351 ± 40. [ ] – Mean age.

Sample number	Grains counted	Fossil tracks Tracks/cm² (x10⁵)	Fossil tracks #Tracks counted	Induced tracks Tracks/cm² (x10⁶)	Induced tracks #Tracks counted	Age (standard error) (Ma)	95% Confidence limits (Ma)	CHI² (%)	Uranium content (ppm)	Mean track length (s.e.) (μm)	N
88NAC01	20	2.26	111	1.23	607	45.8 (5.4)	58 36	98	15	13.4 (0.4)	64
88NAC02	20	3.62	443	2.30	2822	39.4 (3.0)	46 33	50	27	13.6 (0.3)	102
88NAC04	12	0.23	14	0.42	210	44.4 (12.7)	78 25	99	3	12.4 (0.9)	10
88NAC05	20	4.42	387	2.50	2183	44.9 (3.5)	52 38	98	27	13.8 (0.3)	110
88NAC06	20	3.00	239	0.93	748	80.8 (7.5)	97 67	99	12	13.0 (0.4)	102
88NAC07	7	1.04	23	1.91	210	43.4 (9.8)	68 27	90	15	-	-
88NAC08	20	2.73	176	1.33	859	52.2 (5.2)	64 43	99	15	13.4 (0.3)	102
88NAC09	20	2.70	139	1.23	634	56.0 (6.1)	70 45	95	15	12.6 (0.4)	102
88NAC10	20	1.64	135	0.71	590	58.6 (6.4)	73 47	99	9	12.7 (0.3)	102
88NAC11	20	3.20	260	1.53	1246	53.6 (4.7)	64 45	7	18	12.2 (0.4)	101
88NAC12	5	4.96	62	2.80	350	45.6 (6.8)	61 34	99	30	-	-
88NAC13	20	1.92	180	1.22	1151	[65.4] [7.7]	81 50	<5	12	13.7 (0.4)	74
88NAC15	20	5.03	433	1.90	1634	[65.9] [3.9]	74 58	<5	21	12.8 (0.5)	101
88NAC16	20	3.45	174	1.44	728	62.2 (6.3)	76 51	75	15	11.1 (0.5)	100
89NAC17	20	1.37	82	1.92	575	56.1 (7.2)	72 43	>99	15	-	-
89NAC18	20	1.03	95	2.00	924	40.5 (4.8)	51 32	>99	15	13.6 (1.1)	6
89NAC19	20	0.92	48	1.89	491	38.4 (6.1)	53 28	>99	15	-	-
89NAC20	17	1.69	88	2.93	761	45.5 (5.6)	58 35	92	21	-	-
89NAC21	20	0.65	74	1.24	707	41.2 (5.5)	54 32	>99	9	13.9 (0.6)	7
89NAC23	20	1.48	71	3.50	839	33.1 (4.4)	43 25	99	24	13.4 (0.5)	53

Bishop Lodge Member found adjacent to the Santa Fe Range was derived from the underlying Proterozoic rocks (Galusha and Blick, 1971), suggesting that at least part of the Santa Fe block was at the surface in the Miocene. Denny (1940) noted that the Santa Fe Group near Santa Fe does not contain copious quantities of coarse-grained sediments, which is indicative of a source to the east of the modern range boundary. Denny (1940) proposed that the Santa Fe Group may have extended as far east as the modern summits of the Sangre de Cristo Mountains.

Sandia Mountains—Kelley and Duncan (1986) determined apatite FT ages for the Sandia Mountains (Fig. 12), an east-tilted fault block of Proterozoic crystalline and Paleozoic to Mesozoic sedimentary rocks. The apparent FT ages generally range from 30 ± 5 Ma at high elevation to 14 ± 4 Ma at low elevation. Track-length measurements for the three highest-elevation samples were presented by Kelley and Duncan (1986). Since we are now using a different track-length measuring system, we have re-analyzed the three highest-elevation samples. In addition, we have determined the track-length distributions for the other eleven samples from the Sandia Mountains, and the results are presented in Table 6. The time–temperature curves derived from the track-length and age data indicate that cooling rates for this mountain range during the late Oligocene to middle Miocene are on the order of 7 to 12°C/Ma (Fig. 13).

The track-length measurements presented in Table 6 for 81SANO1 and 02 are quite different from those shown by Kelley and Duncan (1986) because more tracks were measured in this study (75 to 101 versus 20). The two highest-elevation samples, which are located in the Proterozoic granite just below the Paleozoic section, are young compared to the other high-elevation samples (Fig. 14). Hot water moving laterally along the contact between the granite and the sedimentary rocks in a manner similar to that observed at the hot dry rock site in the Jemez Mountains (GT-1, Fig. 9; Harrison et al., 1986) may have totally annealed the tracks in apatite in the top part of the granite. This event occurred

TABLE 6—Track length data summary for samples of Kelley and Duncan (1986).

Sample	Apatite FT age (Ma)	Standard error (Ma)	# of tracks measured	Measured mean (microns)	Standard deviation (microns)	95% confidence interval (microns)
			Santa Fe Range			
81SF01	55.1	6.1	28	13.5	1.6	0.6
81SF02	57.4	5.3	25	13.0	2.0	0.8
81SF03	55.6	5.7	89	13.8	1.6	0.3
81SF04	59.0	4.6	51	13.9	1.6	0.4
81SF05	61.6	6.7	50	13.4	2.1	0.6
81SF06	61.0	4.3	77	13.6	1.4	0.3
81SF07	59.4	5.1	100	13.9	1.7	0.3
81SF08	68.2	7.1	50	13.8	1.7	0.5
81SF09	74.0	6.1	38	13.8	1.6	0.5
81SF10	57.6	5.3	50	13.8	1.9	0.5
81SF11	62.0	5.3	100	13.7	1.8	0.4
81SF12	64.6	5.3	-	-	-	-
81SF13	62.9	7.5	50	13.8	1.2	0.3
81SF14	69.3	10.0	40	13.4	1.8	0.5
81SF15	63.7	8.3	50	13.4	1.7	0.5
81SF16	43.8	5.2	30	13.4	2.3	0.8
			Sandia Mountains			
81SAN01	21.5	2.0	101	14.8	1.7	0.3
81SAN02	20.2	2.3	75	14.3	2.3	0.5
81SAN03	30.4	2.5	100	14.8	1.4	0.3
81SAN04	24.6	2.2	100	15.0	1.8	0.3
81SAN05	23.2	2.4	100	14.7	1.1	0.2
81SAN06	20.3	2.1	100	14.5	1.3	0.2
81SAN07	19.8	1.9	100	13.9	2.0	0.4
81SAN08	17.5	2.1	100	14.4	1.6	0.3
81SAN09	18.8	2.2	100	14.1	2.0	0.4
81SAN10	14.2	1.9	70	14.1	2.7	0.6
81SAN12	18.6	2.4	16	13.0	2.5	1.2
81SAN13	15.2	1.3	100	14.0	1.8	0.4
81SAN14	18.7	1.7	50	14.5	1.3	0.4
81SAN15	22.6	2.4	51	14.2	2.6	0.7
			Taos Range			
81WP01	34.2	5.9	66	14.6	1.4	0.3
81WP02	25.1	4.1	100	14.9	1.4	0.3
81WP04	22.9	3.6	100	14.2	1.8	0.4
81WP05	21.8	3.6	100	13.0	3.3	0.6
81WP06	21.3	3.6	100	11.9	4.2	0.8
81WP07	18.5	3.4	70	13.5	3.4	0.8
WP08 (Lucero)	17.6	3.6	-	-	-	-
81WP09	26.9	5.0	68	13.5	2.9	0.7

in the early Miocene (about 21 to 22 Ma). The remainder of the section seems to have been unaffected by the groundwater movement.

Central New Mexico

Much of the effort in this study has been devoted to determining FT ages in the mountain ranges that flank the southern Albuquerque Basin, since the transition in structural style from primarily single, en-echelon half-grabens in the northern rift to several subparallel half-grabens in the southern rift occurs in this area. Generally, the apatite FT ages for the ranges on the west side of the west-dipping southern Albuquerque Basin half-graben are younger than the ages on the east side.

Manzano–Los Pinos Mountains—The rocks exposed in the Manzano–Los Pinos (M–LP) chain (Fig. 12) include Proterozoic crystalline rocks that were juxtaposed across high-angle reverse faults with Pennsylvanian and Permian sed-

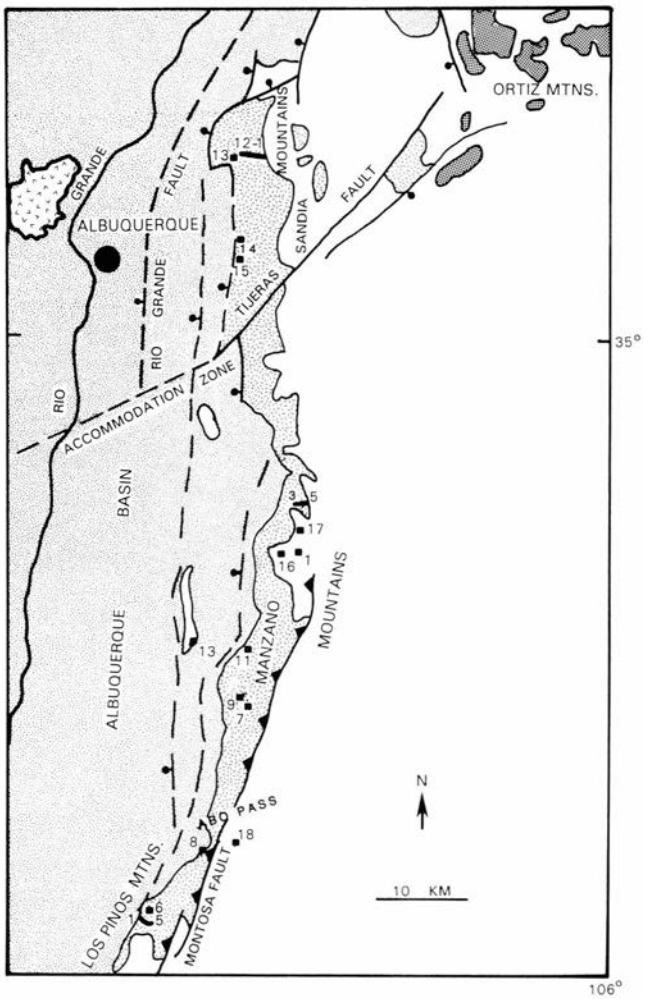

FIGURE 12—Generalized geologic map of the east side of the Albuquerque Basin (Woodward et al., 1978). Ages in Sandia Mountains are from Kelley and Duncan (1986). Sample numbers are shown on the map, FT data for Manzano and Los Pinos Mountains are in Table 6.

imentary rocks during the Laramide orogeny. The Manzanita and Manzano Mountains are separated from the Sandia Mountains on the north by the Tijeras fault, a major strike—slip fault that has been reactivated several times since the Proterozoic, and from the Los Pinos Mountains on the south by a canyon at Abo Pass (Fig. 12). A low-angle normal fault that is possibly a reactivated Laramide thrust fault has been identified along the western margin of the chain from an interpretation of a COCORP seismic line through Abo Pass (de Voogd et al., 1986).

Apatite FT ages for Pennsylvanian sedimentary rocks, the Proterozoic Ojito Granodiorite and Proterozoic metasediments and metavolcanics in the Manzano Mountains, vary from 23 ± 5 Ma to 46 ± 7 Ma and show good correlation with elevation (Fig. 14). The Ojito Granodiorite is the only sampled rock unit in the Manzano Mountains that contains apatite with abundant confined tracks. The cooling history derived from apatite in the Ojito Granodiorite (Fig. 15) shows that the high-elevation portions of the Manzano Mountains cooled at a rate of about 3 to 4°C/Ma between 30 and 10 Ma. Mean track lengths of 12.3 to 12.9 p.m with standard deviations of 2.0 to 2.9 p.m for other rock units in the Manzano Mountains imply similar histories. Data from the higher elevations of the range suggest that these rocks were brought to shallow levels in the crust during Laramide deformation and subsequent Eocene erosion. The samples then cooled at relatively slow rates compared to the Sandia Mountains and other ranges bordering the southern Albuquerque Basin during the early phases of rift formation. The cooling history of the low-elevation samples is poorly constrained due to the low apatite and uranium content of the meta-sediments exposed on the west side of the range. The data from 88MAN11 and 88MAN12 were combined in order to improve the error analysis for these two samples, which were collected approximately 100 m from each other in the same rock unit (shown as 11 in Fig. 12). The combined date of 22.9 ± 4.7 Ma for the low-elevation samples is indicative of cooling during early rift formation.

One sample, 88MAN13, was collected from the Hubbell bench (Fig. 12), a shallow bench within the Albuquerque Basin adjacent to the west side of the Manzano Mountains (Kelley, 1977). This sample from the Permian Yeso Forma-

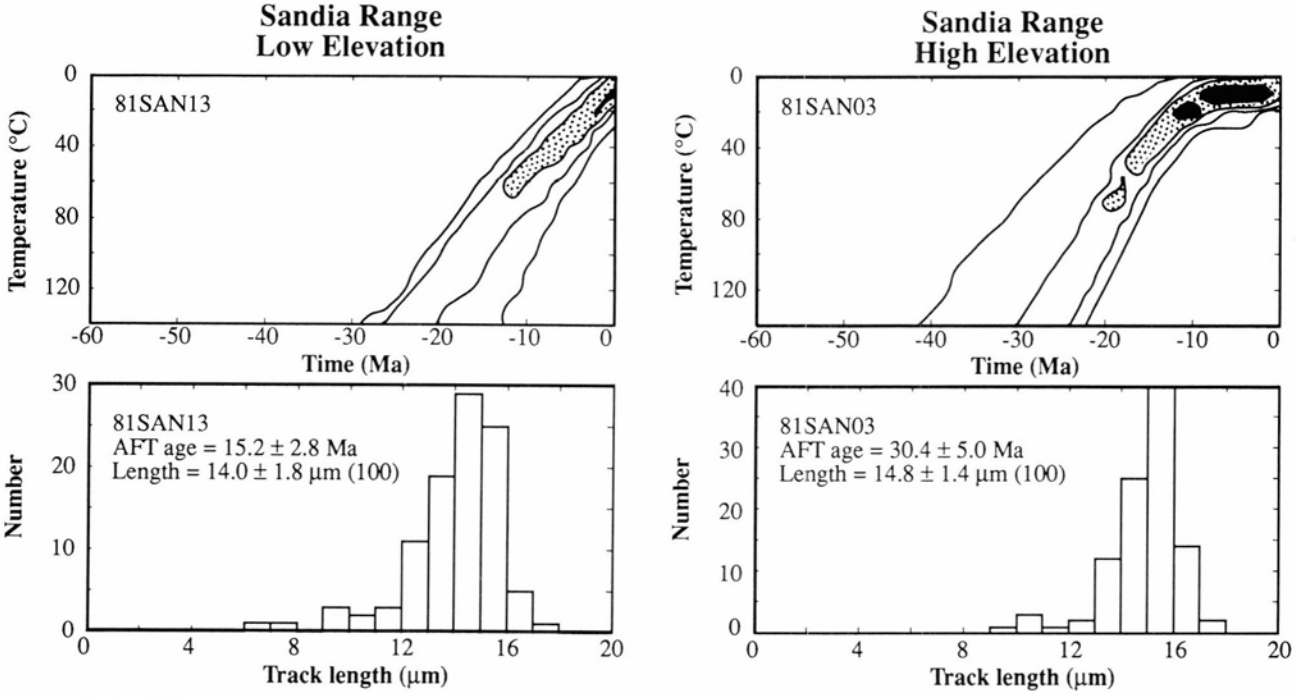

FIGURE 13—Representative track-length distributions and thermal histories for samples from the Sandia Mountains.

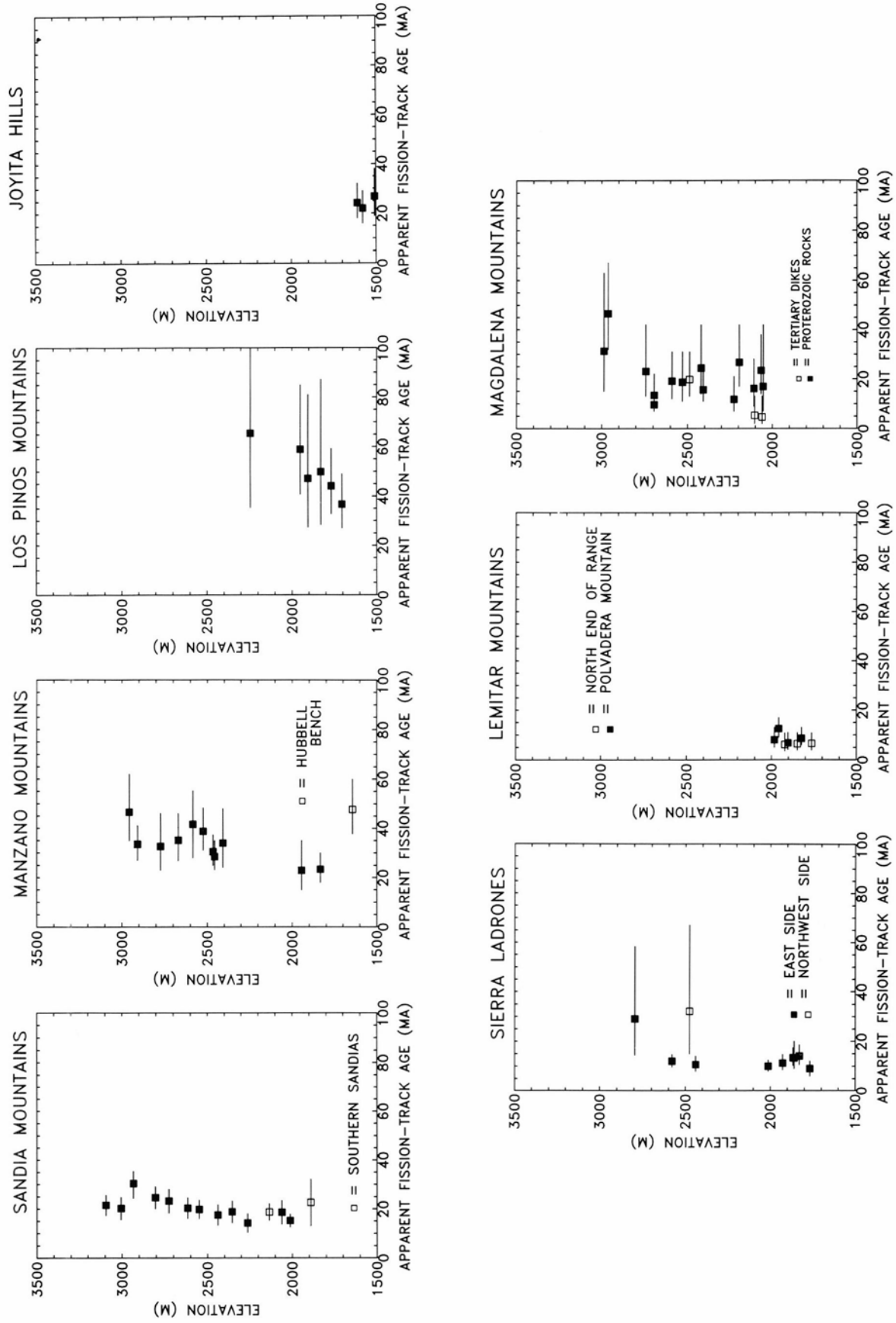

FIGURE 14—Age versus elevation plots for mountain ranges in central Rio Grande rift.

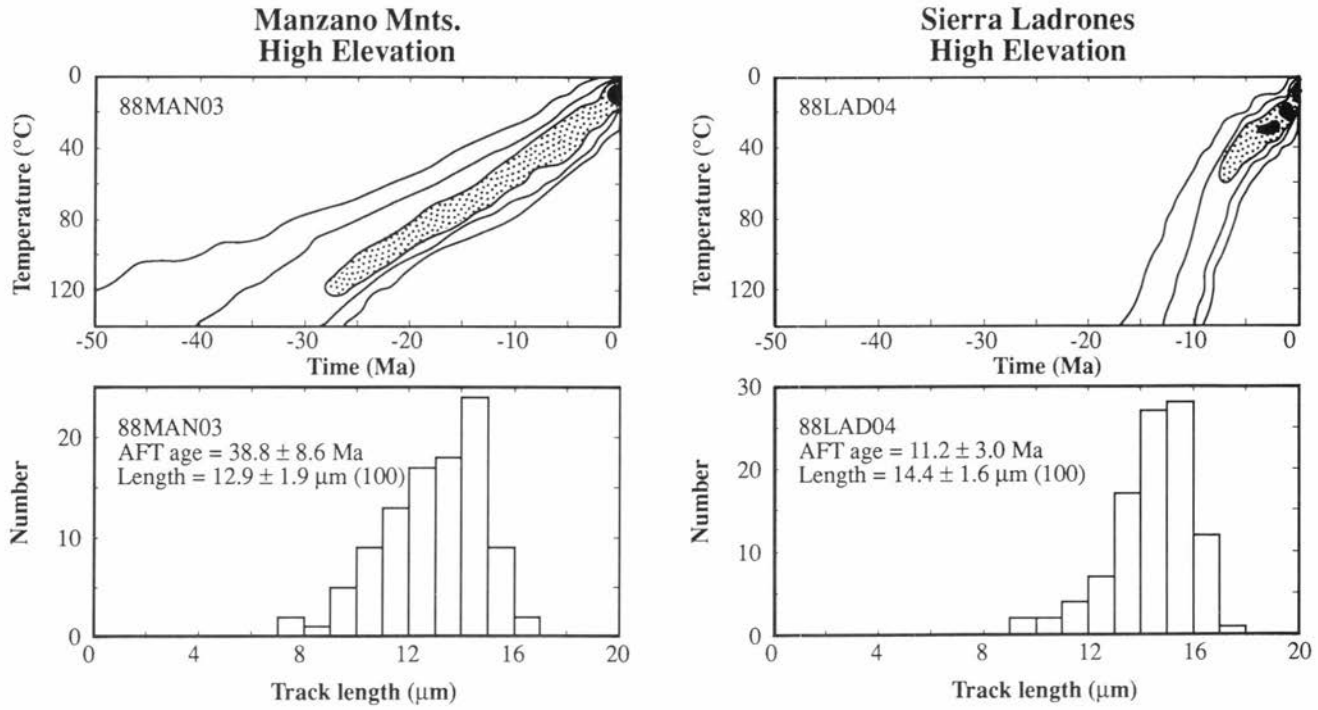

FIGURE 15—Representative track-length distributions and thermal histories for samples from the Manzano Mountains and the Sierra Ladrones.

tion yielded an age of 48 ± 11 Ma and a mean length of 13.2 ± 2.0 again recording Eocene erosion. Rocks exposed in the Hubbell bench were apparently downfaulted into the basin and preserved from erosion beneath a shallow cover of Santa Fe Group sediments. Unfortunately, since the compositional range of the well-rounded apatite is so large (Table 2), no modeling of the sample's thermal history could be done; however, qualitative analysis suggests slow cooling (about 3°C/Ma).

The thermal histories extracted from the FT data are consistent with the depositional history of the southeastern Albuquerque Basin. The sediments deposited in this area record a denudation event that involved erosion of late Paleozoic sedimentary rocks in the Eocene or late Oligocene to early Miocene from a source region in the vicinity of the modern Manzano Mountains (Lozinsky, 1988). No significant amount of Proterozoic detritus appears to have been derived from the Manzano-Sandia Mountain area until 10 to 12 Ma, when there is an influx of Proterozoic rock fragments into the upper Popotosa Formation (Lozinsky, 1988). Deposition in the past 5 Ma in the southeastern part of the basin has been dominated by material eroded from the Manzano uplift.

The ages from the Los Pinos Mountains (Fig. 12) range from 37 ± 5 to 65 ± 20 Ma (Fig. 14), recording Laramide uplift and Eocene erosion. The ages show good correlation with elevation. Unfortunately, the uranium content of the fluorapatite in the Precambrian Los Pinos Granite is low (<5.0 ppm), so very few confined tracks were found and statistically meaningful track-length measurements were not possible. However, the large age range over a short vertical distance suggests that this block cooled slowly (about 1 to 3°C/Ma).

Joyita Hills—The Joyita Hills (Fig. 15) are a northwest-tilted block of low topographic relief that lies within the Rio Grande rift. The block is made up of Proterozoic granite overlain by a thick (approximately 2100 to 2400 m) section of Pennsylvanian to Cretaceous sedimentary rocks and Cenozoic volcanic and sedimentary units. The youngest ash flow tuff that covers this area has an 40Ar/39Ar age of 27.36 ± 0.07 Ma (McIntosh et al., 1990; Osburn and Chapin, 1983). The block is bounded on the east by the enigmatic East Joyita fault, which separates Proterozoic rocks on the west from Cenozoic volcanic rocks on the east. A melange of Proterozoic to Cenozoic rocks is present along the fault and in places the fault is intruded by a rhyolitic dike. The western boundary of the block is buried beneath the late Cenozoic sediments of the Santa Fe Group.

FT ages from Proterozoic granite in the Joyita Hills increase progressively to the west, from 22 to 27 Ma, consistent with the westward tilt of the block. Few confined tracks were found in the apatite from these granites, but generally the mean length is 13.6 to 13.7 ± 0.9 to 1.4 µm, suggesting intermediate (4 to 5°C/Ma) cooling rates during early rift extension in the late Oligocene and early Miocene. Evidence for uplift of the Joyita Hills in the late Oligocene to early Miocene is also found in the sedimentary record in the southeastern Albuquerque Basin. Volcanic and volcaniclastic rock fragments derived from a source in the vicinity of the Joyita Hills are found in the lower Popotosa Formation of early to middle Miocene age (Lozinsky, 1988). Detritus from this area is also found in the upper Popotosa Formation.

The Joyita Hills block is a southern extension of the Hubbell bench; the elevations of both areas are comparably low (1643 m for sample 88MAN13 from the Hubbell bench and 1509 to 1610 m for the three samples from the Joyita Hills). The FT data support the interpretations of DeVoogd et al. (1986) and Russell and Snelson (1990) that the Hubbell benchJoyita Hills block has been downfaulted into the Albuquerque Basin and rotated on the upper plate of a west-dipping listric normal fault. The older FT age of 48 Ma for the Permian Yeso in the Hubbell bench characterizes the cooling history of the stratigraphically high portions of the block, while the younger ages on the Proterozoic granites in the Joyita Hills constrain the thermal history of stratigraphically lower levels of the block.

Sierra Ladrones—The Sierra Ladrones, which lie on the

southwestern margin of the southern Albuquerque Basin, occupy a significant position in the rift. To the north and east of the range the rift is approximately 80 km wide, but immediately south of the range the rift widens to 130 km (Lewis, 1989). The uplift consists of west-tilted Proterozoic granitic and metamorphic rocks overlain by a dip-slope of Paleozoic limestones on the west side. The block is bounded on three sides by Cenozoic normal faults: it is bordered on the east by the east-dipping, low-angle (about 26°) Jeter fault, on the west by the high-angle Ladron fault, and on the southeast by the high-angle Cerro Colorado fault (Fig. 16). The presence of Oligocene volcanic rocks from volcanic centers to the south in small fault blocks on the north and east sides of the range indicates that significant topography did not exist in the region during the Oligocene.

The apparent fission-track ages along the eastern margin of the Sierra Ladrones are 9 ± 2 to 14 ± 2 Ma (Fig. 14) over the entire elevation range sampled. The track-length histograms for these samples are unimodal, with mean lengths of 14.0 to 14.8 p.m and standard deviations of 1.1 to 1.6 p.m. These data indicate that the east side of the Sierra Ladrones cooled rapidly, on the order of 12 to 20°C/Ma. The cooling history for 88LAD04 shown in Fig. 15 is representative of the data from the east side of the range.

In contrast to the samples from the east side of the range, two samples from the northwest side and from Ladron Peak (89LAD08, 89LAD11) are older, with FT ages of 32 ± 12 Ma and 29 ± 10 Ma, respectively. No confined tracks were found in the extremely low-uranium (<3 ppm) apatite. The position of these samples in the block suggests significant rotation to the west. This rotation is supported by structures in the overlying Paleozoic sedimentary rocks.

The timing of this uplift is consistent with the sedimentary record. Lower Santa Fe Group in the southwestern

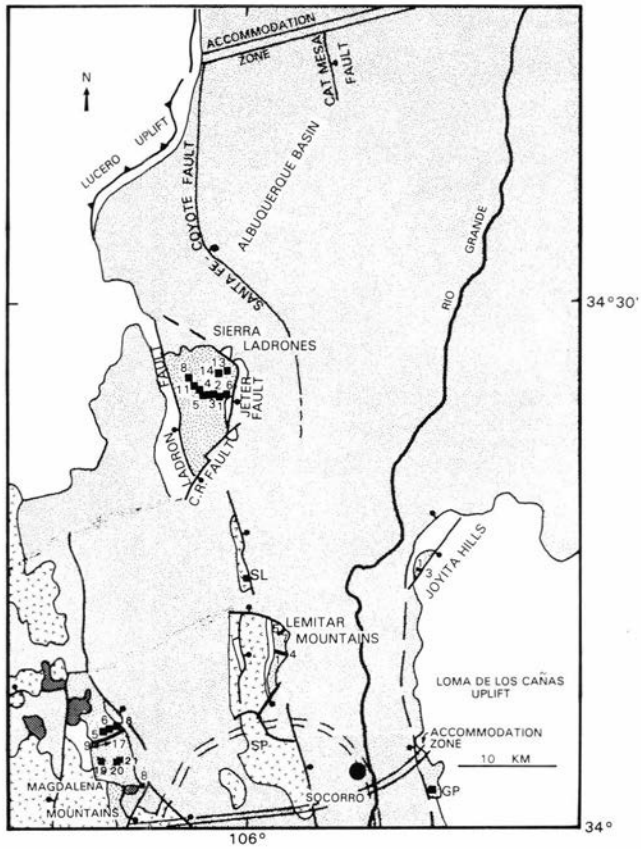

FIGURE 16—Generalized geologic map of the south end of the Albuquerque Basin (Woodward et al., 1978). Sample numbers are shown on the map, FT data are in Table 7.

Albuquerque Basin contains primarily sedimentary and volcanic rock fragments, while the upper Santa Fe Group, which was largely deposited in the past 5 Ma, includes a mixture of granitic, metamorphic, sedimentary, and volcanic rock fragments (S. M. Cather, pers. comm. 1991). During much of deposition of the lower Santa Fe Group, the rocks sampled in this study were at depths of 2 to 3 km; the Proterozoic rocks reached the surface after deposition of a 14.55 ± 0.04 Ma ($^{40}Ar/^{3}9Ar$ age; W. C. McIntosh, unpubl. data) ash bed within the Santa Fe Group.

Wernicke and Axen (1988) and Lewis (1989) proposed that Sierra Ladrones represents an isostatically uplifted footwall of a detachment related to the east-dipping, low-angle Jeter fault. The FT data support this interpretation; furthermore, the FT data imply that the structures exposed at the surface formed within the zone of brittle deformation. Preliminary zircon FT ages from the Sierra Ladrones are Mesozoic (143 to 211 Ma). Typically, crustal temperatures must exceed at least 300°C for the ductile deformation observed in core complexes to form (Ord and Hobbs, 1989). The zircon FT data indicate that these rocks were not at temperatures above 240°C during Tertiary extension. Thus the apatite and zircon data suggest that the Tertiary deformation preserved in the Sierra Ladrones occurred at shallow crustal levels (3 to 6 km). The preservation of a thick Paleozoic carbonate section on the west-tilted dip slope of the range also indicates that the exposed Proterozoic rocks represent the uppermost Proterozoic section

Lemitar Mountains—Oligocene to early Miocene strata sitting on older rocks in the Lemitar Mountains (Fig. 16) have been strongly rotated to the west along east-dipping, low-angle faults (Chamberlin, 1983). Based on the relationship between faulting and Oligocene ash-flow tuffs affected by the faulting, Chamberlin (1983) proposed that the faults started out as high-angle faults when extension began at approximately 30 Ma, and that the faults subsequently rotated to a low-angle configuration. The low-angle faults were later cut by high-angle faults, which were again rotated. Both the subhorizontal late Oligocene to early Miocene faults and the moderately east-dipping middle to late Miocene faults have been cut by a third generation of high-angle faults. Palinspastic reconstruction indicates that the amount of extension in this range may be as high as 200% (Chamberlin, 1983).

FT samples were collected along two traverses through Proterozoic rocks in the footwall of middle to late Miocene faults along the east side of the Lemitar Mountains (Fig. 16). The FT ages from the central portion of the block range from 7 to 12 Ma and show weak correlation with elevation (Fig. 14). The sampling traverse essentially parallels the projection of one of the subhorizontal faults. The FT ages for all three samples from the north end of the range are 6 to 7 Ma. Few confined tracks were observed due to the young age and low uranium content of the samples, but the few that were found are long (14.3 ± 0.8 p.m). The FT data are consistent with rapid cooling related to the formation of the middle to late Miocene set of faults. However, part of the cooling may be related to the waning of volcanism in the Socorro area. The block lies on the northern margin of the 12 to 7 Ma Socorro Peak rhyolite field (Chamberlin, 1980; Bobrow et al., 1983; Chapin, 1989). The apatite FT ages are similar to the age of the rhyolitic volcanism, which suggests that the FT data reflect the combined effects of uplift and changes in heat flow related to volcanism.

Magdalena Mountains—The Magdalena Mountains (Fig. 16) consist primarily of 20 to 40 Ma volcanic rocks that were generally erupted from several overlapping, nested cauldrons (Chapin et al., 1978; Osburn and Chapin, 1983). The volcanic rocks overlie Proterozoic crystalline rocks and Paleozoic sedimentary rocks. This area is of interest because

synrift sediments of the latest Oligocene to Miocene Popotosa Formation (Santa Fe Group) crop out on the crest of the range at an elevation of 3230 m, indicating substantial uplift since basin formation in the late Oligocene (Chapin et al., 1978).

Samples were collected from Proterozoic intrusive, metavolcanic, and metasedimentary rocks. The Proterozoic Magdalena Granite contains fluorite rather than apatite, so no FT dates were obtained for this unit. Apatite ages from metavolcanic and metasedimentary rocks range from 10 to 46 Ma. The oldest ages (>30 Ma) are at high elevation, but ages <30 Ma show no correlation with elevation. The ages < 30 Ma do show a correlation as a function of proximity to Tertiary rhyolite and quartz-monzonite dikes. A zircon FT age of 27.9 ± 1.5 Ma was determined for one of the quartz-monzonite dikes; monzonitic to granitic stocks in the northern Magdalena Mountains have K/Ar ages of 28 to 31 Ma (Chapin, 1989). The rhyolite dikes have not been dated. Both the quartz-monzonite and rhyolite dikes have been affected by quartz—sericite alteration (Sumner, 1980). The apatite FT ages from the Proterozoic rocks adjacent to the dikes suggest that hydrothermal alteration of some of the dikes in the northern part of the range occurred 10 to 12 Ma, perhaps during circulation of hydrothermal fluids associated with rhyolite volcanism along the southeastern flank of the Magdalena Range and at Socorro Peak (10 to 15 km to the east). The rhyolite volcanism occurred between 7.2 and 12.1 Ma in the Socorro Peak area and at 10.8 to 12.1 Ma along the southeastern margin of the range (Chapin, 1989). Slightly older rhyolitic volcanism occurred between 13.5 and 18.4 Ma along the west side of the Magdalena Mountains (Chapin, 1989).

The FT data suggest that some of the high-elevation samples in the Magdalena Mountains cooled during Eocene erosion, but the Eocene erosion ages have been modified by subsequent hydrothermal activity. As in the Sandia Mountains, the highest-elevation sample taken from just beneath the Paleozoic limestones capping the range is younger (89MAG09, 31.3 Ma) than the adjacent lower-elevation sample (89MAG10, 46.5 Ma; Fig. 14). The younger age may be due to circulation of hydrothermal fluids through the extensively mineralized Mississippian Kelly Limestone that rests on Proterozoic rocks. The mineralization is thought to be related to stock intrusions dated at 28 to 31 Ma (Chapin et al., 1978). Samples at low elevations away from the direct influence of Tertiary dikes have early to middle Miocene (16 to 19 Ma) ages. Unfortunately, the apatite yields and uranium contents of the apatite from this area are low; therefore, few confined tracks were observed (Table 7) and no thermal modeling was attempted.

TABLE 7—Apatite fission-track ages for central Rio Grande rift, New Mexico. Zeta = 351 ± 40.

Sample number	Grains counted	Fossil tracks		Induced tracks		Age (standard error) (Ma)	95% Confidence limits (Ma)	CHI^2 (%)	Uranium content (ppm)	Mean track length (s.e.) (μm)	N
		$Tracks/cm^2$ ($x10^5$)	#Tracks counted	$Tracks/cm^2$ ($x10^6$)	#Tracks counted						
					Manzano Mountains						
88MAN01	20	1.82	158	2.76	1198	30.5 (3.1)	37 25	99	36	13.8 (0.5)	82
88MAN03	20	2.38	128	2.85	766	38.8 (4.3)	48 31	99	36	12.9 (0.4)	100
88MAN04	20	1.93	150	3.16	1226	28.5 (2.9)	35 23	97	39	12.8 (0.5)	100
88MAN05	20	0.58	43	0.80	295	34.0 (5.9)	48 24	98	9	13.0 (0.5)	89
88MAN07	20	1.10	77	1.47	515	35.1 (4.7)	46 27	99	18	11.3 (2.0)	5
88MAN09	20	0.78	68	0.80	346	46.5 (6.7)	62 35	99	9	12.4 (0.7)	29
88MAN11	20	0.35	20	0.82	236	20.1 (4.8)	32 12	93	9	-	-
88MAN12	20	0.09	6	0.10	41	34.9 (15.3)	84 14	99	3	-	-
88MAN13	20	2.98	117	2.48	586	47.7 (5.5)	60 38	99	30	13.2 (0.5)	71
89MAN16	20	1.06	133	2.20	1384	33.5 (3.5)	41 27	97	18	14.1 (0.4)	43
89MAN17	20	0.74	38	1.60	403	32.6 (5.8)	46 23	99	12	14.0 (0.6)	21
89MAN18	20	1.22	78	3.60	1153	23.4 (3.0)	30 18	99	30	14.2 (0.5)	30
					Los Pinos Mountains						
88LP01	20	1.31	64	1.35	329	44.1 (6.5)	59 33	99	15	-	-
88LP02	14	0.22	16	0.20	73	49.8 (14.0)	87 28	99	3	-	-
88LP03	8	1.00	17	0.96	82	47.1 (12.8)	81 27	98	12	-	-

Table 7 continued

Sample number	Grains counted	Fossil tracks Tracks/cm^2 (x10^5)	Fossil tracks #Tracks counted	Induced tracks Tracks/cm^2 (x10^6)	Induced tracks #Tracks counted	Age (standard error) (Ma)	95% Confidence limits (Ma)	CHI^2 (%)	Uranium content (ppm)	Mean track length (s.e.) (μm)	N
88LP05	20	0.14	14	0.10	49	65.4 (20.0)	121 35	99	3	-	-
88LP06	20	0.81	41	0.63	160	53.9 (10.8)	85 41	94	6	-	-
89LP08	20	0.52	58	1.14	636	35.7 (5.3)	49 27	99	9	-	-
					Joyita Hills						
90JOY01	20	0.54	39	1.36	491	26.8 (4.7)	38 19	99	12	13.6 (0.6)	10
90JOY02	20	0.82	67	2.26	925	24.2 (3.3)	32 18	99	18	13.6 (0.9)	5
90JOY03	20	0.80	61	2.44	929	22.0 (3.1)	29 16	99	21	13.7 (0.6)	18
					Sierra Ladrones						
88LAD01	20	1.01	136	4.08	2752	12.0 (1.2)	15 10	95	48	14.5 (0.2)	100
88LAD02	20	0.85	59	3.94	1357	10.6 (1.5)	14 8	40	48	14.6 (0.3)	100
88LAD03	20	0.89	116	4.38	2846	10.0 (1.1)	12 8	60	51	14.5 (0.3)	100
88LAD04	20	0.71	71	3.08	1541	11.2 (1.5)	15 9	79	36	14.4 (0.3)	100
88LAD05	20	1.01	75	3.68	1374	13.4 (1.8)	17 10	81	42	14.8 (0.3)	53
88LAD06	20	0.91	64	3.18	1116	14.1 (2.0)	19 11	81	36	14.0 (0.4)	50
88LAD08	40	0.11	8	0.27	100	32.2 (11.9)	67 15	95	3	-	-
90LAD11	15	0.21	9	0.57	120	29.1 (10.1)	58 14	99	3	-	-
90LAD13	20	0.30	43	2.24	1595	9.0 (1.5)	12 6	99	18	14.5 (1.1)	10
90LAD14	20	0.24	29	1.23	736	13.3 (2.6)	20 9	99	12	-	-
					Lemitar Mountains						
90LEM01	20	0.45	46	1.24	1266	12.5 (2.0)	17 9	99	12	-	-
90LEM02	20	0.24	20	1.05	864	8.0 (1.8)	13 5	85	9	-	-
90LEM03	20	0.17	17	1.74	890	6.7 (1.7)	11 4	99	15	-	-
9OLEM04	20	0.21	25	1.72	1032	8.6 (1.8)	13 6	97	15	-	-
90LEM05	20	0.16	13	2.01	823	6.1 (1.7)	11 4	99	15	-	-
90LEM06	20	0.22	15	2.67	907	6.4 (1.7)	11 4	30	21	-	-
90LEM07	20	0.26	16	3.08	957	6.5 (1.7)	11 4	80	24	-	-
					Magdalena Mountains						
88MAG05	20	0.37	22	0.70	205	26.7 (6.2)	42 17	98	6	-	-
88MAG06	20	0.37	15	0.70	232	16.1 (4.4)	28 9	80	12	12.0 (2.2)	11

Table 7 continued

Sample number	Grains counted	Fossil tracks: Tracks/cm^2 (x10^5)	Fossil tracks: #Tracks counted	Induced tracks: Tracks/cm^2 (x10^6)	Induced tracks: #Tracks counted	Age (standard error) (Ma)	95% Confidence limits (Ma)	CHI^2 (%)	Uranium content (ppm)	Mean track length (s.e.) (μm)	N
88MAG07	28	0.24	5	1.17	125	16.9 (7.8)	42 7	80	9	-	-
89MAG08	20	0.46	19	1.59	327	23.4 (5.6)	38 14	85	12	-	-
89MAG09	15	0.26	9	0.57	96	31.3 (11.0)	63 15	92	6	-	-
89MAG10	9	1.85	37	2.63	263	46.5 (8.4)	67 32	96	24	-	-
89MAG11	20	0.91	40	6.26	1377	9.6 (1.6)	13 7	99	54	14.6 (0.7)	9
89MAG12	40	0.06	16	0.31	396	13.4 (3.5)	22 8	98	3	-	-
89MAG13	40	0.22	19	0.76	326	19.1 (4.6)	31 12	99	6	-	-
89MAG14	30	0.18	17	0.64	299	18.7 (4.7)	31 11	99	6	-	-
89MAG15	40	0.22	32	0.92	673	15.6 (2.9)	23 11	99	9	-	-
89MAG16	40	0.10	13	0.57	361	11.7 (3.3)	21 7	97	6	-	-
89MAG17	20	0.04	5	0.63	364	5.3 (2.4)	13 2	70	6	-	-
89MAG18	20	0.04	4	0.80	335	4.6 (2.3)	13 2	50	6	-	-
90MAG19	20	0.18	12	0.96	327	23.0 (6.8)	42 13	99	3	-	-
90MAG20	20	0.22	15	1.13	386	24.4 (6.5)	42 14	99	6	-	-
90MAG21	20	0.30	21	1.90	666	19.8 (4.4)	31 13	99	9	15.0 (1.5)	12
					Gonzales Prospect						
90GP01	20	0.25	3	0.24	142	8.2 (4.8)	26 3	40	3	-	-
					San Lorenzo Canyon						
90SL01	20	0.039	5	0.38	245	12.8 (5.8)	32 5	99	3	-	-

Isolated Proterozoic outcrops: Gonzales Prospect and San Lorenzo Canyon—Several knobs of Proterozoic granites are located on the western margin of the Loma de las Cañas uplift (Fig. 16). One of the most prominent outcrops in this area is associated with the Gonzales fluorite prospect. The apatite FT age of granite from this outcrop is 8.2 ± 4.8 Ma, which probably reflects the age of fluorite mineralization.

A small exposure of Proterozoic granite and schist is located north of San Lorenzo Canyon, which runs along the northern end of the Lemitar Mountains (Fig. 16). A thin section of Paleozoic sedimentary rocks and a thick section of Tertiary volcanic rocks lie above the granite. The apatite FT age of 12.8 ± 5.8 Ma for this granite is similar to FT results from the Lemitar Mountains to the south and the Sierra Ladrones to the north.

Summary of FT results from the central rift—The FT data show that the east flank of the rift at this latitude has not been strongly uplifted during rifting, allowing preservation of rocks that cooled during late Eocene erosion. The lowest-elevation samples in the Manzano Mountains and the ages from the Joyita Hills reflect cooling following the waning of volcanism and uplift related to extension in latest Oligocene to early Miocene. Cooling rates on the east side of the rift are on the order of 1 to 4°C/Ma.

Uplift of the Manzano and Los Pinos Mountains was sufficient, however, to remove relatively thin layers of Cenozoic volcanic rocks that once covered this region. In contrast, most of the mountain ranges within the rift and along its western flank still have thick volcanic sections derived from sources in the Mogollon-Datil volcanic field. Exceptions are Ladron Peak and the northern Magdalena Range, where Proterozoic rocks are now exposed at elevations as high as 2923 m. Only in the highest-elevation samples of the Magdalena Mountains do we see any evidence of the preservation of Eocene ages on the west side of the rift. Elsewhere on the west side of the central rift FT ages are dominantly Miocene and cooling rates are rapid (10 to 20°C/Ma). The Miocene FT ages in the Lemitar and Magdalena Mountains are controlled to some degree by elevated heat flow related to volcanism in the 7 to 12 Ma Socorro Peak

rhyolite field and the 13 to 18 Ma Magdalena Peak rhyolite field. The Sierra Ladrones are far enough from these volcanic centers not to be directly affected by this thermal event.

The southern portion of the Albuquerque—Belen Basin is a half-graben tilted down to the west (Russell and Snelson, 1990; Chapin, 1988). Young apatite FT ages, high cooling rates, and high degrees of extension are found on the deep side of the half-graben; major boundary-fault displacement has occurred on the west side of the basin, causing isostatic uplift of the footwall blocks. Interestingly, major volcanism during the Oligocene to early Miocene and minor volcanism during middle to late Miocene also occurs on the west side of the rift. Intrusions in the crust most likely preferentially weakened it and concentrated fault activity on the west side of this portion of the rift (Morgan et al., 1986; Dunbar and Sawyer, 1989).

Discussion

Tectonic history based on FT analysis

The FT data from the northern and central Rio Grande rift clearly show that each mountain block forming the eastern and western margins of the rift has a unique cooling history reflecting the effects of burial, volcanism, and denudation. At least four major tectonic events are recorded by FT data from this area.

(1) The Santa Fe Range, the Los Pinos Mountains, and the eastern margin of the Nacimiento uplift cooled during the early Laramide orogenic event. In the Santa Fe Range cooling rates during the early Laramide are approximately 1 to 3°C/Ma. The cooling history of the Los Pinos Mountains is not well constrained, but this block is estimated to have cooled slowly (1 to 3°C/Ma). Cooling rates in the eastern Nacimiento Mountains are on the order of 1°C/Ma. The preservation of older ages in these areas implies that subsequent denudation was not vigorous, or that these rocks were protected from deep erosion by overlying middle Tertiary sedimentary and volcanic units.

(2) Remnants of areas that cooled during late Laramide deformation and during late Eocene erosion have been preserved at high elevation in the La Veta Pass area, Culebra Range, Taos Range (Wheeler Peak; Kelley, 1990) portions of the Sangre de Cristo Mountains, and in the Nacimiento, Manzano, and Magdalena Mountains. Cooling rates during this interval are typically 2 to 4°C/Ma.

(3) Areas with apatite FT ages in the 10 to 25 Ma range have thermal histories controlled by the effects of volcanism and/or denudation associated with the early phase of rift development. In two areas with 10 to 25 Ma FT ages, the Sawatch Range and the lower elevation portion of the Taos Range, the samples were taken directly from late Eocene to Oligocene intrusives. The samples record the effects of geothermal systems (Sawatch Range) or late intrusions (Taos Range; Kelley, 1990) superimposed on denudation of the early rift intrusives. Two other areas with Oligocene to Miocene ages, the La Veta Pass—Culebra Range part of the Sangre de Cristo Mountains and the Magdalena Mountains, lie near sites of extensive Oligocene to early Miocene volcanism, the San Juan—Latir and the Mogollon—Datil volcanic fields, respectively. In these cases, the effects of relaxation of isotherms following regional volcanism are hard to separate from those of denudation.

Mountain blocks along the rift where denudation rather than volcanism is thought to dominate the cooling history during the Oligocene to early Miocene include the northern Sangre de Cristo Mountains, Blanca Peak, Sandia Mountains, and Sierra Ladrones. Cooling rates in the northern Sangre de Cristo Mountains based on the work of Lindsey et al. (1986) are about 5 to 9°C/Ma. This block is bounded on two sides by faults that have been active in the late Cenozoic. Blanca Peak, with a cooling rate of 12°C/Ma, is outlined on three sides by young normal faults. The Sandia Mountains generally cooled at rates of 7 to 12°C/Ma; this block is bounded on the north and west by rift-related normal faults and on the south by a major strike—slip fault. The Sierra Ladrones, which is surrounded on three sides by normal faults, cooled at 12 to 20°C/Ma and was rotated to the west during this interval. The rapid denudation that occurred in these four blocks reflects the isostatic response of the footwall during fault-related unloading on two or three sides of these blocks.

(4) Areas with apatite FT ages between 5 to 10 Ma include the eastern margin of the Sawatch Range, the Mosca Pass area, the promontory near San Luis in the Sangre de Cristo Mountains, and the Lemitar Mountains. These FT ages reflect the combined effects of hydrothermal activity (Sawatch, San Luis), volcanism (Lemitar), and denudation. Cooling rates during the late phase of rift formation are high (5 to 15°C/Ma).

A correlation between the overall apparent apatite FT age range of a mountain block and the tilt of the adjacent half-graben is observed at several places along the rift (Fig. 17). Generally, the younger FT ages are found in the mountain ranges adjacent to the deep side of the half-grabens. Faults along the deep side of the half-grabens commonly have large amounts of displacement. For example, the Santa Fe—Coyote fault on the west side of the southern Albuquerque Basin has 3050 m of throw, and the Cat Mesa fault just east of the Santa Fe—Coyote fault has 4500-5200 m of throw (Russell and Snelson, 1990); these faults are near the Sierra Ladrones, the site of rapid rift-related uplift and erosion. North of the Tijeras accommodation zone, major fault displacement occurs on the Rio Grande fault, which lies on the east side of the rift valley. The Rio Grande fault has a throw of 4500 to 6100 m (Russell and Snelson, 1990). This fault bounds the Sandia Mountains, another block with rapid rift-related uplift and erosion. Similarly, in the northern San Luis Basin young ages in the northern Sangre de Cristo Mountains are found adjacent to the major graben-controlling fault which has 4000 to 5000 m of displacement (Brister and Gries, in press). Thus the mountain blocks with young FT ages reflect an isostatic response to large-scale displacements along the major half-graben bounding faults.

As discussed above, the cooling rates derived from the FT data have increased through time. Examination of the cooling curves from areas with Laramide ages reveals that between 60 and 40 Ma the samples typically cooled 40°C, which corresponds to a maximum of about 2 km of uplift and erosion associated with this event, assuming geothermal gradients on the order of 20°C/km. The total amount of denudation is less if a higher gradient is assumed. These results imply that the preserved remnants of Laramide uplifts did not have great topographic relief. In contrast, cooling curves for areas with middle Miocene ages show that there is commonly a temperature drop of 60 to 90°C between 15 and 5 Ma, which is equivalent to 2 to 3 km of uplift and erosion during rift development, assuming a constant gradient of 30°C/km. Estimated denudation rates during rifting in areas largely unaffected by late Tertiary volcanism are on the order of 200 to 300 m/Ma. Similar amounts of denudation during the peak of extensional activity have been noted by Bohannon et al. (1989) and Omar et al. (1989) in the Red Sea rift and by Brown et al. (1990) along the southwestern coast of Africa.

A histogram of our new FT ages is shown in Fig. 18. In addition to our ages, we have included FT ages for the northern-rift flanks from Kelley and Duncan (1986), Lindsey et al. (1986), Bryant and Naeser (1980), Shannon (1988), and Lipman et al. (1986). The distribution of ages gives a temporal overview of the cooling of rocks through the 60 to 120°C range. Cooling is controlled by a number of mecha-

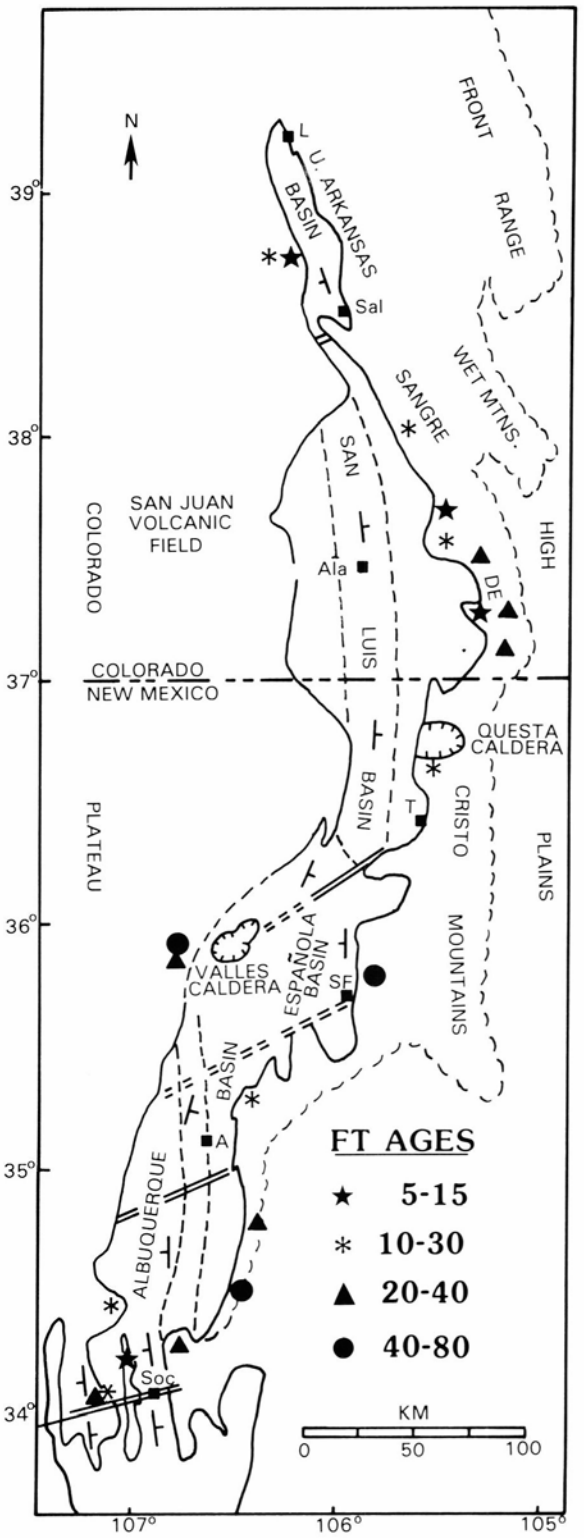

FIGURE 17—Regional map summarizing the generalized apatite FT age ranges for each mountain block in the northern and central Rio Grande rift. Base map from Chapin (1988). Each symbol represents the main period of cooling, but there is considerable overlap. The stars are assigned to areas where hydrothermal activity related to the late phase of rifting dominates the cooling history. Areas with asterisks cooled during early rifting at rates greater than 5°C/Ma. The triangles represent areas that generally cooled at rates below 5°C/Ma and/or areas where late Eocene ages are preserved at high elevation. The solid circles signify areas where rocks that cooled during the Laramide orogeny are preserved. Since the Joyita Hills are structurally related to the Hubbell bench, the age range for this intrarift block is considered to be 22 to 48 Ma (see text for discussion).

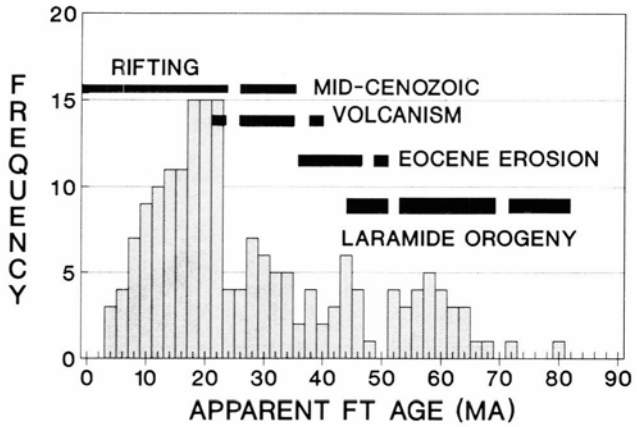

FIGURE 18—Histogram of FT ages from this study, Kelley and Duncan (1986), Lindsey et al. (1986), Bryant and Naeser (1980), Shannon (1988), and Lipman et al. (1986).

nisms, including uplift and denudation, rotation, and relaxation of isotherms following volcanism. The age distribution is also affected by differential preservation of rocks, lack of exposure of rocks that have cooled but have not reached the surface, and annealing of fission tracks by elevation of isotherms due to hydrothermal activity or burial. In spite of the large number of variables, the three broad peaks on the histogram appear to fit the tectonic evolution of the Rio Grande rift region as deduced from other studies. The oldest peak (80 to 52 Ma) represents rocks that cooled during Laramide uplift. The population of ages older than 66 Ma has undoubtedly been much reduced by erosion; consequently, most of the cooling ages in this peak are late Laramide. The second peak (48 to 28 Ma) represents rocks that cooled during the latest Laramide uplift, carving of the late Eocene erosion surface, or the beginning of rifting. These rocks are generally found in the highest elevations of mountain ranges. The third peak (24 to 8 Ma) represents rocks that cooled during block faulting of the margins of the rift basins and/or lowering of isotherms following the peak of Oligocene volcanism.

The lack of ages younger than 5 Ma reflects the lag between the time cooling commenced at depths of 2 to 3 km and the time the rocks reach the surface (i.e. these rocks are still in the subsurface). The scarcity of ages between 56 and 48 Ma and between 28 and 24 Ma may indicate inadequate sampling or perhaps periods of relative stability when neither rocks nor isotherms were moving significantly, so that fewer cooling ages were generated.The 28 to 24 Ma lull may also reflect peak geothermal gradients that developed during the 29 to 26 Ma climax of ignimbrite volcanism, which may have caused rising isotherms and annealing of tracks in previously cooled rocks. The interpretation of the lulls is speculative at this point, but it will be interesting to see if this pattern persists with further sampling.

Models for uplift of rift flanks

One type of thermomechanical model that has been applied directly to the Rio Grande rift involves the thermal and isostatic consequences of the thinning of the lithosphere and upwelling of the asthenosphere during extension (Bridwell and Anderson, 1980). This type of model typically produces a maximum of about 1 km of uplift during the late phase of rifting (Morgan, 1991), which is significantly less than the 2 to 3 km of denudation indicated by the FT data. Morgan (1991) proposed that it is possible to get as much as 6 km of uplift by thickening the crust during extension through magmatic underplating. In addition, phase changes in the upper mantle and lower crust during lithospheric heating can lead to uplift (Morgan, 1991).

The models discussed above do not specifically address the asymmetry observed in the topography of the rift flanks, the structure of the half-grabens, and the amount of uplift implied by the FT data in the Rio Grande rift. The asymmetry of topographic and structural features has been recognized in other rift basins and in continental margins by many authors and has been summarized by Chapin (1988). Many mechanical models have been developed to examine the origin of the asymmetry. Instead of explaining rift-flank uplifts strictly in terms of thermal phenomena, recent work has focused on the flexural isostatic response of the lithosphere to faulting and denudation. Typically, the uplift adjacent to a single large fault is considered in these models (Buck et al., 1988; Weissel and Karner, 1989; King and Ellis, 1990). While flexural uplift has not been directly investigated in the Rio Grande rift, this type of modeling has been successfully applied to explain topographic and gravity data from another young rift, the Rhine graben (Weissel and Karner, 1989). Flexural isostasy has also been used to match the topography and the amount of uplift predicted by FT results in a mature passive margin (Gilchrist and Summerfield, 1990).

In summary, near-surface features such as asymmetric and rotated structures, large local relief, and the amount of denudation predicted from FT results are not easily modeled with large-scale thermomechanical models, but are more readily explained in terms of localized isostatic flexures (Buck et al., 1988; Wernicke and Axen, 1988). A more detailed analysis of flexural isostasy needs to be applied to the Rio Grande rift to see if this mechanism is consistent with geologic, geophysical, and geochronological data.

Acknowledgments

Support for this project was provided by NSF grant EAR-8804203 and by the New Mexico Bureau of Mines & Mineral Resources. David Lindsey generously provided his Sangre de Cristo samples to us for analysis. Thanks to Roger Phillips for collecting the Sawatch Range samples; Ted Stans for allowing us into the Los Pinos Mountains and Joyita Hills on the Sevilleta Wildlife Refuge; and David Blackwell, Chris Beck, Steve Bergman, Steve Cather, and Charles Naeser for helpful discussions. The Corning glasses were provided by Jan Schreurs of Corning Glass Works. David Crouch helped with the mineral separations. Sample irradiations were done at the Texas A&M Nuclear Science Center and were funded under the DOE Reactor Share Program.

References

Aldrich, M. J., Jr., Chapin, C. E., and Laughlin, A. W., 1986, Stress history and tectonic development of the Rio Grande rift, New Mexico: Journal of Geophysical Research, v. 91, pp. 6199-6211.

Baltz, E. H., 1967, Stratigraphy and regional tectonic implications of part of Upper Cretaceous and Tertiary rocks, east-central San Juan Basin, New Mexico: U.S. Geological Survey, Professional Paper 552, 101 pp.

Bobrow, D. J., Kyle, P. R., and Osbum, G. R., 1983, Miocene rhyolitic volcanism in the Socorro area of New Mexico: New Mexico Geological Society, Guidebook 34, pp. 211-217.

Bohannan, R. G., Naeser, C. W., Schmidt, D. L., and Zimmermann, R. A., 1989, The timing of uplift, volcanism, and rifting peripheral to the Red Sea: A case for passive rifting?: Journal of Geophysical Research, v. 94, pp. 1683-1701.

Bridwell, R. **J.,** and Anderson, C. A., 1980, Thermomechanical models of the Rio Grande rift; *in* Davies, E. E., and Runcorn, S. K. (eds.), Mechanisms of Continental Drift and Plate Tectonics: NATO Advanced Study Institute, Newcastle-upon-Tyne, England, pp. 41-59.

Brister, B. S., and Gries, R. R., in press, Tertiary stratigraphy and tectonic development of the Alamosa Basin, Rio Grande rift, south-central Colorado; *in* Keller, G. R., and Cather, S. M. (eds.), Basins of the Rio Grande rift: Structure, stratigraphy and tectonic setting: Geological Society of America, Memoir.

Brookins, D. G., Forbes, R. B., Turner, D. L., Laughlin, A. W., and Naeser, C. W., 1977, Rb–Sr, K–Ar, and fission-track geochronological studies of samples from the LASL drill holes GT1, GT-2, and EE-1: Los Alamos National Laboratories, Report LA-6829-MS, 22 pp.

Brown, R. W., Rust, D. J., Summerfield, M. A., Gleadow, A. J. W., and DeWit, M. C. J., 1990, An Early Cretaceous phase of accelerated erosion on the southwestern margin of Africa: Evidence from apatite fission track analysis and the offshore sedimentary record: Nuclear Tracks and Radiation Measurements, v. 17, pp. 339-350.

Bryant, B., and Naeser, C. W., 1980, The significance of fission-track ages of apatite in relation to the tectonic history of the Front Range and Sawatch Range, Colorado: Geological Society of America, Bulletin, Part I, v. 91, pp. 156-164.

Buck, W. R., Martinez, F., Steckler, M. S., and Cochran, J. R., 1988, Thermal consequences of lithospheric extension: Pure and simple: Tectonics, v. 7, pp. 213-234.

Carlson, W. D., 1990, Mechanisms and kinetics of apatite fission-track annealing: American Mineralogist, v. 75, pp. 1120-1139.

Chamberlin, R. M., 1980, Cenozoic stratigraphy and structure of the Socorro Peak volcanic center, central New Mexico: A summary: New Mexico Geology, v. 3, pp. 22-24.

Chamberlin, R. M., 1983, Cenozoic domino-style crustal extension in the Lemitar Mountains, New Mexico: A summary: New Mexico Geological Society, Guidebook 34, pp. 111-118.

Chapin, C. E., 1988, Axial basins of the northern and central Rio Grande rift; *in* Sloss, L. L. (ed.), Sedimentary Cover—North American Craton: Geological Society of America, Decade of North American Geology, D-2, Chapter 8, pp. 165-170.

Chapin, C. E., 1989, Volcanism along the Socorro accommodation zone, Rio Grande rift, New Mexico: New Mexico Bureau of Mines & Mineral Resources, Memoir 46, pp. 46-57.

Chapin, C. E., and Seager, W. R., 1975, Evolution of the Rio Grande rift in the Socorro and Las Cruces areas: New Mexico Geological Society, Guidebook 26, pp. 297-321.

Chapin, C. E., Chamberlin, R. M., Osburn, G. R., Sanford, A. R., and White, D. W., 1978, Exploration framework of the Socorro geothermal area, New Mexico: New Mexico Geological Society, Special Publication 7, pp. 115-130.

Church, S. E., and Bickford, M. E., 1971, Spontaneous fission-track studies of accessory apatite from granitic rocks in the Sawatch Range, Colorado: Geological Society of America, Bulletin, v. 82, pp. 1727-1734.

Corrigan, J. D., 1991, Deriving thermal history information from apatite fission-track data: Journal of Geophysical Research, v. 96, pp. 10347-10360.

Corrigan, J. D., in press, Apatite fission-track analysis of Oligocene strata in south Texas: Testing annealing models: Chemical Geology.

Crowley, K. D., in press, Mechanisms and kinetics of apatite fission-track annealing: Discussion: American Mineralogist.

Crowley, K. D., Cameron, M., and Schaefer, **R.** L., 1991, Experimental studies of annealing of etched fission tracks in fluorapatite: Geochemica et Cosmochimica Acta, v. 55, pp. 1449-1465.

Cunningham, C. G., Naeser, C. W., and Marvin, R. F., 1977, New ages for intrusive rocks in the Colorado mineral belt: U.S. Geological Survey, Bulletin 1395-C, 7 pp.

Denny, C. S., 1940, Santa Fe Formation in the Espanola Valley, New Mexico: Geological Society of America, Bulletin, v. 51, pp. 677-694.

Donelick, R. A., 1988, Etchable fission track-length reduction in apatite: Experimental observations, theory, and geological applications: Unpublished PhD dissertation, Rensselaer Polytechnic Institute, Troy, New York, 414 pp.

Dunbar, J. A., and Sawyer, D. S., 1989, How preexisting weaknesses control the style of continental breakup: Journal of Geophysical Research, v. 94, pp. 7278-7292.

deVoogd, B., Brown, L. D., and Merey, C., 1986, Nature of the eastern boundary of the Rio Grande rift from COCORP surveys

in the Albuquerque Basin, New Mexico: Journal of Geophysical Research, v. 91, pp. 6305-6320.
Duddy, I. R., Green, P. F., and Laslett, G. M., 1988, Thermal annealing of fission tracks in apatite, 3. Variable temperature behavior: Chemical Geology (Isotope Geoscience Section), v. 73, pp. 25-38.
Epis, R. C., and Chapin, C. E., 1975, Geomorphic and tectonic implications of the post-Laramide late Eocene erosion surface in the Southern Rocky Mountains: Geological Society of America, Memoir 144, pp. 45-74.
Galbraith, R. F, 1981, On statistical models for fission track counts: Journal of Mathematical Geology, v. 13, pp.471-478.
Galbraith, R. F., and Laslett, G. M., 1985, Some remarks on statistical estimation in fission-track dating: Nuclear Tracks, v. 10, pp. 361-363.
Galusha, T., and Blick, J. C., 1971, Stratigraphy of the Santa Fe Group, New Mexico: American Museum of Natural History, Bulletin 144, 127 pp.
Gilchrist, A. R., and Summerfield, M. A., 1990, Differential denudation and flexural isostasy in formation of rifted-margin upwarps: Nature, v. 346, pp. 739-742.
Gleadow, A. J. W., and Duddy, I. R., 1981, A natural long-term annealing experiment for apatite: Nuclear Tracks, v. 5, pp.169-174.
Gleadow, A. J. W., Duddy, I. R., Green, P. F., and Lovering, J. F., 1986, Confined fission-track lengths in apatite—a diagnostic tool for thermal history analysis: Contributions to Mineralogy and Petrology, v. 94, pp. 405-415.
Green, P. F., 1985, A comparison of zeta calibration baselines in zircon, sphene, and apatite: Chemical Geology (Isotope Geoscience Section), v. 58, pp. 1-22.
Green, P. F., Duddy, I. R., Laslett, G. M., Hegarty, K. A., Gleadow, A. J. W., and Lovering, J. F, 1989, Thermal annealing of fission tracks in apatite 4. Quantitative modelling techniques and extension to geological timescales: Chemical Geology (Isotope Geoscience Section), v. 79, pp. 155-182.
Green, P. F., 1988, The relationship between track shortening and fission track age reduction in apatite: Combined influences of inherent instability, annealing anisotropy, length bias, and system calibration: Earth and Planetary Science Letters, v. 88, pp. 335-352.
Green, P. F., Duddy, I. R., Gleadow, A. J. W., Tingate, P. R., and Laslett, G. M., 1986, Thermal annealing of fission tracks in apatite, 1. A qualitative description: Chemical Geology (Isotope Geoscience Section), v. 59, pp. 237-253.
Harrison, T. M., Morgan, P., and Blackwell, D. D., 1986, Constraints on the age of heating at the Fenton Hill site, Valles caldera, New Mexico: Journal of Geophysical Research, v. 91, pp. 1899-1908.
Hurford, A. J., and Green, P. F., 1983, The zeta age calibration of fission-track dating: Isotope Geoscience, v. 1, pp. 285-317. Jones, D. M., and Benson, R. G., 1990, The San Luis (El Plomo) gold deposit, Costilla County, Colorado: New Mexico Geological Society, Guidebook 41, pp. 14-15.
Kearney, B. C., 1983, Volcanic stratigraphy and structure of the La Veta Pass area, northern Sangre de Cristo Mountains, south-central Colorado: Unpublished MS thesis, Southern Methodist University, Dallas, Texas, 67 pp.
Kelley, S. A., 1990, Late Mesozoic to Cenozoic cooling history of the Sangre de Cristo Mountains, Colorado and New Mexico: New Mexico Geological Society, Guidebook 41, pp. 123-132. Kelley, S. A., and Duncan, I. J., 1986, Late Cretaceous to middle Tertiary tectonic history of the northern Rio Grande rift: Journal of Geophysical Research, v. 91, pp. 6246-6262.
Kelley, V. C., 1977, Geology of the Albuquerque Basin: New Mexico Bureau of Mines & Mineral Resources, Memoir 33, 60 pp.
Knepper, D. H., 1976, Late Cenozoic structure of the Rio Grande rift zone, central Colorado: Colorado School of Mines, Professional Contributions, v. 8, pp. 421-430.
King, G., and Ellis, M., 1990, The origin of large local uplift in extensional regions: Nature, v. 348, pp. 689-693.
Laslett, G. M., Green, P. F., Duddy, I. R., and Gleadow, A. J. W., 1987, Thermal annealing of fission tracks in apatite, 2. A quantitative analysis: Chemical Geology (Isotope Geosciences Section), v. 65, pp. 1-13.
Lewis, C. J., 1989, Crustal extension and shoulder uplift in the Rio Grande rift, New Mexico: Half-grabens and accommodation zones in the Ladrones Peak area: Unpublished MS thesis, California State University, Los Angeles, 78 pp.
Lindsey, D. A., Andriessen, P. A. M., and Wardlaw, B. R., 1986, Heating, cooling, and uplift during Tertiary time, northern Sangre de Cristo Range, Colorado: Geological Society of America, Bulletin, v. 97, pp. 1133-1143.
Lipman, P. W., 1975, Evolution of the Platoro caldera complex and related volcanic rocks, southeastern San Juan Mountains, Colorado: U.S. Geological Survey, Professional Paper 852, 128 pp. Lipman, P. W., 1981, Volcano-tectonic setting of Tertiary ore deposits: Arizona Geological Society Digest, v. 14, pp. 199-211.
Lipman, P. W., Mehnert, H. H., and Naeser, C. W., 1986, Evolution of the Latir volcanic field, northern New Mexico, and its relation to the Rio Grande rift, as indicated by potassium-argon and fission track dating: Journal of Geophysical Research, v. 91, pp. 6329-6346.
Lozinsky, R. P., 1988, Stratigraphy, sedimentology, and sand petrology of the Santa Fe group and pre-Santa Fe Tertiary deposits in the Albuquerque Basin, central New Mexico: Unpublished PhD dissertation, New Mexico Institute of Mining & Technology, **Socorro,** 298 pp.
McIntosh, W. C., Sutter, J. F., Chapin, C. E., and Kedzie, L. L., 1990, High-precision 40Ar39Ar sanidine geochronology of ignimbrites in the Mogollon-Datil volcanic field, southwestern New Mexico: Bulletin of Volcanology, v. 52, pp. 584-601.
Morgan, P., 1991, Neogene magmatism, extension, uplift, and lithosphere evolution in the Rio Grande rift (abs.): Geological Society of America, Abstracts with Programs, v. 23, p. 51.
Morgan, P., Seager, W. R., and Golombek, M. P., 1986, Cenozoic thermal, mechanical, and tectonic evolution of the Rio Grande rift: Journal of Geophysical Research, v. 91, pp. 6263-6276.
Naeser, C. W., 1979, Fission-track dating and geologic annealing of fission tracks; *in* Jager, E., and Hunziker, J. C. (eds.), Lectures in Isotope Geology: Springer-Verlag, New York, pp. 154-169.
Olson, H. J., and Dellechaie, F., 1976, The Mount Princeton geothermal area, Chaffee County, Colorado: Colorado School of Mines, Professional Contributions, v. 8, pp. 431-438.
Olson, J. C., Marvin, R. F., Parker, R. L., and Mehnert, H. H., 1977, Age and tectonic setting of lower Paleozoic alkalic and mafic rocks, carbonatites, and thorium veins in south-central Colorado: U.S. Geological Survey, Journal of Research, v. 5, pp. 673-687. Omar, G. I., Steckler, M. S., Buck, W. R., and Kohn, B. P., 1989, Fission-track analysis of basement apatites at the western margin of the Gulf of Suez rift, Egypt: Evidence for synchroneity of uplift and subsidence: Earth and Planetary Science Letters, v. 94, pp. 316-328.
Ord, A., and Hobbs, B. E., 1989, The strength of the continental crust, detachment zones and the development of plastic instabilities: Tectonophysics, v. 158, pp. 269-289.
Osburn, G. R., and Chapin, C. E., 1983, Nomenclature for Cenozoic rocks of northeast Mogollon-Datil volcanic field, New Mexico: New Mexico Bureau of Mines & Mineral Resources, Stratigraphic Chart 1.
Parrish, R. R., 1983, Cenozoic thermal evolution and tectonics of the Coast Mountains of British Columbia, 1. Fission track dating, apparent uplift rates and pattern of uplift: Tectonics, v. 2, pp. 601-632.
Russell, L. R., and Snelson, S., 1990, Structural style and tectonic evolution of the Albuquerque basin segment of the Rio Grande rift; *in* Pinet, B., and Bois, C. (eds.), The Potential of Deep Seismic Profiling in Hydrocarbon Exploration: Edition Technit, Paris, pp. 175-207.
Shannon, J. R., 1988, Geology of the Mount Aetna cauldron complex, Sawatch Range, Colorado: Unpublished PhD dissertation, Colorado School of Mines, Golden, 434 pp.
Shannon, J. R., Epis, R. C., Naeser, C. W., and Obradovich, J. D., 1987, Correlations of intracauldron and outflow tuffs and an intrusive tuff dike related to the Oligocene Mount Aetna cauldron, central Colorado; *in* Drexler, J. W., and Larson, E. E. (eds.), Cenozoic Volcanism in the Southern Rocky Mountains Revisited: Colorado School of Mines Quarterly, v. 82, pp. 65-80.
Sharp, W. N., 1970, Extensive zeolitization associated with hot springs in central Colorado: U.S. Geological Survey, Professional Paper 700-B, pp. 14-20.
Smith, R. P., 1979, Early rift magmatism at Spanish Peaks, Colorado; *in* Riecker, R. E. (ed.), Rio Grande Rift: Tectonics and Magmatism: American Geophysical Union, Washington, D.C., pp. 313-321.
Smith, L. N., 1991, Laramide sedimentation and tectonics of the

SE San Juan Basin (abs.): Geological Society of America, Abstracts with Programs, v. 23, p. 95.
Steven, T. A., 1975, Middle Tertiary volcanic field in the southern Rocky Mountains: Geological Society of America, Memoir 144, pp. 75-94.
Sumner, W., 1980, Geology of the Water Canyon—Jordan Canyon area, Socorro County, New Mexico: Unpublished MS thesis, New Mexico Institute of Mining & Technology, Socorro, 143 pp. Tweto, 0., 1979, The Rio Grande rift system in Colorado; *in* Riecker, R. E. (ed.), Rio Grande Rift: Tectonics and Magmatism: American Geophysical Union, Washington, D.C., pp. 33-56.
Tweto, 0., 1978, Tectonic map of the Rio Grande rift system in Colorado: New Mexico Bureau of Mines & Mineral Resources, Circular 163, Sheet 1.
Vrolijk, P., Donelick, R. A., Queng, J., and Cloos, M., in press, Testing of fission track annealing in apatite in a simple thermal setting: Site 800, ODP leg 129: Proceedings of the Ocean Drilling Project, Scientific Results.
Weissel, J. K., and Kamer, G. D., 1989, Flexural uplift of rift flanks due to mechanical unloading of the lithosphere during extension: Journal of Geophysical Research, v. 94, pp. 13919-13950.
Wernicke, B., and Axen, G. J., 1988, On the role of isostacy in the evolution of normal fault systems: Geology, v. 16, pp. 848-851.
Woodward, L. A., 1987, Geology and mineral resources of Sierra Nacimiento and vicinity, New Mexico: New Mexico Bureau of Mines & Mineral Resources, Memoir 42, 84 pp.
Woodward, L. A., Callender, J. F., Seager, W. R., Chapin, C. E., Gries, J. C., Shaffer, W. L., and Zilinski, R.E., 1978, Tectonic map of Rio Grande rift region in New Mexico, Chihuahua, and Texas: New Mexico Bureau of Mines & Mineral Resources, Circular 163, Sheet 2.

Appendix starts on next page.

Appendix

Sample localities and descriptions

Sample	Latitude	Longitude	Elevation (m)	Rock type
		Sawatch Range		
84MP01	38°43.04'	106°13.39'	2640	Mt. Princeton Granite (Eocene)
84MP02	38°44.52'	106°12.04'	3146	Mt. Princeton Granite (Eocene)
84MP03	38°44.53'	106°11.57'	3055	Mt. Princeton Granite (Eocene)
84MP04	38°44.57'	106°11.19'	2969	Mt. Princeton Granite (Eocene)
84MP05	38°44.91'	106°11.24'	2899	Mt. Princeton Granite (Eocene)
84MP06	38°44.55'	106°21.09'	3896	Mt. Princeton Granite (Eocene)
84MP07	38°44.48'	106°20.96'	3846	Mt. Princeton Granite (Eocene)
84MP08	38°44.40'	106°20.78'	3747	Mt. Princeton Granite (Eocene)
84MP09	38°43.14'	106°20.65'	3396	Mt. Princeton Granite (Eocene)
84MP10	38°42.36'	106°20.39'	3041	Mt. Princeton Granite (Eocene)
84MP11	38°42.38'	106°18.05'	2902	Mt. Princeton Granite (Eocene)
84MP12	38°42.95'	106°15.34'	2768	Mt. Princeton Granite (Eocene)
		Sangre de Cristo Mountains		
88SG01	37°44.82'	105°27.40'	3299	Gneiss (Proterozoic)
88SG03	37°43.84'	105°27.67'	2927	Granite (Proterozoic)
88SG05	37°44.00'	105°30.36'	2536	Metasediment (Penn. Minturn Fm)
88SG06	37°17.34'	105°09.85'	4121	Sandstone (Penn. Minturn Fm)
88SG07	37°17.87'	105°09.82'	3847	Sandstone (Penn. Minturn Fm)
88SG08	37°19.10'	105°07.65'	3082	Siltstone (Penn-Permian Sangre de Cristo Fm)
88SG09	37°19.92'	105°05.69'	2829	Siltstone (Penn-Permian Sangre de Cristo Fm)

Appendix continued

Sample	Latitude	Longitude	Elevation (m)	Rock type
88SG10	37°36.82'	105°11.34'	2870	Arkose (Penn-Permian Sangre de Cristo Fm)
88SG11	37°31.89'	105°17.69'	2536	Sandstone (Penn. Minturn Fm)
88SG12	37°29.67'	105°20.51'	2530	Gneiss (Proterozoic)
88SG13	37°34.64'	105°29.11'	4373	Gabbro (Proterozoic)
88SG14	37°34.12'	105°30.70'	3591	Gneiss (Proterozoic)
88SG16	37°33.06'	105°33.38'	2732	Granite (Proterozoic)
89SG19	37°17.30'	105°18.70'	2911	Tuff (Oligocene?)
89SG20	37°17.55'	105°16.77'	3280	Granitic Gneiss (Proterozoic)
89SG21	37°17.04'	105°15.49'	3268	Gneiss (Proterozoic)
89SG22	37°14.88'	105°16.71'	3226	Pegmatite Granite (Proterozoic)
89SG23	37°14.24'	105°18.64'	2878	Granitic Gneiss (Proterozoic)
89SG24	37°15.19'	105°19.99'	2646	Quartzite (Proterozoic)
89SG26	37°07.33'	105°11.11'	4283	Granitic Gneiss (Proterozoic)
90SG30	37°36.19'	105°28.52'	3300	Granite (Proterozoic)
90SG31	37°35.69'	105°29.40'	3775	Granite (Proterozoic)
90SG32	37°35.50'	105°28.96'	3525	Granite (Proterozoic)
		Sierra Nacimiento		
88NAC01	35°49.47'	106°50.27'	2508	Granite (Proterozoic)
88NAC02	35°50.55'	106°51.02'	2607	Granite (Proterozoic)
88NAC04	35°46.34'	106°50.63'	2767	Granite (Proterozoic)
88NAC05	35°50.03'	106°51.70'	2706	Granite (Proterozoic)
88NAC06	35°57.00'	106°45.00'	2548	Siltstone (Permian Abo Fm)

Appendix continued

Sample	Latitude	Longitude	Elevation (m)	Rock type
88NAC07	35°59.15'	106°47.34'	2469	Arkose (Penn. Madera Fm)
88NAC08	35°59.80'	106°48.34'	2512	Granite (Proterozoic)
88NAC09	35°59.87'	106°49.40'	2573	Granite (Proterozoic)
88NAC10	35°59.55'	106°52.59'	2366	Siltstone (Permian Abo Fm)
88NAC11	35°59.28'	106°53.59'	2280	Sandstone (Triassic Chinle Fm)
88NAC12	35°58.85'	106°54.89'	2195	Sandstone (Cret. Mesaverde Fm)
88NAC13	35°59.85'	106°55.78'	2186	Sandstone (Cret. Fruitland Fm)
88NAC15	36°02.18'	106°51.25'	2988	Siltstone (Permian Abo Fm)
88NAC16	36°01.59'	106°50.78'	2808	Granite (Proterozoic)
89NAC17	35°54.65'	106°48.57'	2421	Arkose (Permian Abo Fm)
89NAC18	35°57.20'	106°51.71'	2439	Sandstone (Permian Abo Fm)
89NAC19	35°57.16'	106°52.86'	2402	Granite (Proterozoic)
89NAC20	35°56.19'	106°52.99'	2387	Arkose (Permian Abo Fm)
89NAC21	35°41.72'	106°51.51'	2753	Granite (Proterozoic)
89NAC23	35°39.14'	106°51.65'	2119	Granite (Proterozoic)
		Manzano Mountains		
88MAN01	34°46.25'	106°23.55'	2466	Sandstone (Penn. Wild Cow Fm)
88MAN03	34°47.66'	106°23.84'	2524	Granite (Proterozoic)
88MAN04	34°47.63'	106°23.62'	2457	Granite (Proterozoic)
88MAN05	34°47.65'	106°23.49'	2408	Metasediment (Proterozoic)
88MAN07	34°37.67'	106°25.97'	2670	Quartzite (Proterozoic)
88MAN09	34°38.07'	106°26.46'	2957	Gneiss (Proterozoic)
88MAN11	34°40.05'	106°27.64'	1939	Metasediment (Proterozoic)
88MAN12	34°40.21'	106°27.73'	1951	Metasediment (Proterozoic)
88MAN13	34°40.95'	106°33.04'	1643	Siltstone (Permian Yeso Fm)

Appendix continued

Sample	Latitude	Longitude	Elevation (m)	Rock type
89MAN16	34°46.01'	106°25.45'	2908	Sandstone (Penn. Wild Cow Fm)
89MAN17	34°47.38'	106°24.09'	2774	Sandstone (Penn. Los Moyos Fm)
89MAN18	34°26.47'	106°22.51'	1834	Siltstone (Permian Abo Fm)
		Los Pinos Mountains		
88LP01	34°21.27'	106°36.02'	1768	Rhyolite (Proterozoic)
88LP02	34°21.01'	106°35.45'	1829	Granite (Proterozoic)
88LP03	34°20.98'	106°35.32'	1905	Granite (Proterozoic)
88LP05	34°21.43'	106°34.60'	2244	Granite (Proterozoic)
88LP06	34°21.04'	106°35.33'	1951	Basalt (Proterozoic)
89LP08	34°24.23'	106°31.59'	1704	Gneiss (Proterozoic)
		Joyita Hills		
90JOY01	34°16.03'	106°49.80'	1509	Granite (Proterozoic)
90JOY02	34°15.83'	106°49.51'	1610	Granite (Proterozoic)
90JOY03	34°15.66'	106°49.37'	1579	Granite (Proterozoic)
		Sierra Ladrones		
88LAD01	34°25.43'	107°02.34'	1866	Granite (Proterozoic)
88LAD02	34°25.45'	107°03.00'	1927	Granite (Proterozoic)
88LAD03	34°25.55'	107°03.38'	2012	Granite (Proterozoic)
88LAD04	34°25.88'	107°04.84'	2574	Granite (Proterozoic)
88LAD05	34°25.69'	107°04.59'	2439	Granite (Proterozoic)
88LAD06	34°25.65'	107°01.73'	1829	Silicified granite (Proterozoic)
89LAD08	34°26.42'	107°05.55'	2476	Amphibolite (Proterozoic)
90LAD11	34°26.03'	107°05.10'	2796	Felsic tuff (Proterozoic)

Appendix continued

Sample	Latitude	Longitude	Elevation (m)	Rock type
90LAD13	34°28.58'	107°01.48'	1768	Granite (Proterozoic)
90LAD14	34°28.63'	107°02.32'	1860	Granite (Proterozoic)
		Lemitar Mountains		
90LEM01	34°10.81'	106°59.37'	1957	Granite (Proterozoic)
90LEM02	34°10.94'	106°59.19'	1982	Granite (Proterozoic)
90LEM03	34°10.85'	106°59.13'	1902	Granite (Proterozoic)
90LEM04	34°10.77'	106°58.89'	1823	Granite (Proterozoic)
90LEM05	34°11.87'	106°59.39'	1921	Granite (Proterozoic)
90LEM06	34°11.94'	106°58.98'	1847	Granite (Proterozoic)
90LEM07	34°12.17'	106°58.98'	1762	Granite (Proterozoic)
		Magdalena Mountains		
88MAG05	34°04.39'	107°09.68'	2195	Granite (Proterozoic)
88MAG06	34°04.64'	107°09.08'	2109	Metasediment (Proterozoic)
88MAG07	34°04.60'	107°08.53'	2055	Metasediment (Proterozoic)
89MAG08	34°01.55'	107°07.71'	2067	Metasediment (Proterozoic)
89MAG09	34°03.46'	107°10.71'	2988	Dacite tuff (Proterozoic)
89MAG10	34°03.47'	107°10.67'	2963	Dacite tuff (Proterozoic)
89MAG11	34°03.68'	107°10.33'	2695	Gabbro (Proterozoic)
89MAG12	34°03.74'	107°10.29'	2695	Gabbro (Proterozoic)
89MAG13	34°03.86'	107°09.98'	2591	Gabbro (Proterozoic)
89MAG14	34°03.98'	107°09.73'	2530	Gabbro (Proterozoic)
89MAG15	34°04.30'	107°08.92'	2366	Metasediment (Proterozoic)
89MAG16	34°04.53'	107°08.71'	2226	Metasediment (Proterozoic)
90MAG17	34°04.54'	107°08.96'	2104	Monzonite dike (Tertiary)
90MAG18	34°04.85'	107°08.62'	2061	Rhyolite dike (Tertiary)

Appendix continued

Sample	Latitude	Longitude	Elevation (m)	Rock type
90MAG19	34°02.71'	107°10.16'	2743	Dacite tuff (Proterozoic)
90MAG20	34°03.03'	107°08.70'	2421	Felsite tuff (Proterozoic)
90MAG21	34°03.02'	107°08.86'	2488	Monzonite dike (Tertiary)
		Gonzales Prospect		
90GP01	34°04.99'	106°48.32'	1576	Granite (Proterozoic)
		San Lorenzo Canyon		
90SL01	34°14.85'	107°00.41'	1680	Granite (Proterozoic)

Selected conversion factors*

TO CONVERT	MULTIPLY BY	TO OBTAIN
Length		
inches, in	2.540	centimeters, cm
feet, ft	3.048×10^{-1}	meters, m
yards, yds	9.144×10^{-1}	m
statute miles, mi	1.609	kilometers, km
fathoms	1.829	m
angstroms, Å	1.0×10^{-8}	cm
Å	1.0×10^{-4}	micrometers, μm
Area		
in^2	6.452	cm^2
ft^2	9.29×10^{-2}	m^2
yds^2	8.361×10^{-1}	m^2
mi^2	2.590	km^2
acres	4.047×10^{3}	m^2
acres	4.047×10^{-1}	hectares, ha
Volume (wet and dry)		
in^3	1.639×10^{1}	cm^3
ft^3	2.832×10^{-2}	m^3
yds^3	7.646×10^{-1}	m^3
fluid ounces	2.957×10^{-2}	liters, l *or* L
quarts	9.463×10^{-1}	l
U.S. gallons, gal	3.785	l
U.S. gal	3.785×10^{-3}	m^3
acre-ft	1.234×10^{3}	m^3
barrels (oil), bbl	1.589×10^{-1}	m^3
Weight, mass		
ounces avoirdupois, avdp	2.8349×10^{1}	grams, gr
troy ounces, oz	3.1103×10^{1}	gr
pounds, lb	4.536×10^{-1}	kilograms, kg
long tons	1.016	metric tons, mt
short tons	9.078×10^{-1}	mt
oz mt^{-1}	3.43×10^{1}	parts per million, ppm
Velocity		
ft sec^{-1} (= ft/sec)	3.048×10^{-1}	m sec^{-1} (= m/sec)
mi hr^{-1}	1.6093	km hr^{-1}
mi hr^{-1}	4.470×10^{-1}	m sec^{-1}
Pressure, stress		
lb in^{-2} (= lb/in^2), psi	7.03×10^{-2}	kg cm^{-2} (= kg/cm^2)
lb in^{-2}	6.804×10^{-2}	atmospheres, atm
lb in^{-2}	6.895×10^{3}	newtons (N)/m^2, N m^{-2}
atm	1.0333	kg cm^{-2}
atm	7.6×10^{2}	mm of Hg (at 0° C)
inches of Hg (at 0° C)	3.453×10^{-2}	kg cm^{-2}
bars, b	1.020	kg cm^{-2}
b	1.0×10^{6}	dynes cm^{-2}
b	9.869×10^{-1}	atm
b	1.0×10^{-1}	megapascals, MPa
Density		
lb in^{-3} (= lb/in^3)	2.768×10^{1}	gr cm^{-3} (= gr/cm^3)
Viscosity		
poises	1.0	gr cm^{-1} sec^{-1} *or* dynes cm^{-2}
Discharge		
U.S. gal min^{-1}, gpm	6.308×10^{-2}	l sec^{-1}
gpm	6.308×10^{-5}	m^3 sec^{-1}
ft^3 sec^{-1}	2.832×10^{-2}	m^3 sec^{-1}
Hydraulic conductivity		
U.S. gal day^{-1} ft^{-2}	4.720×10^{-7}	m sec^{-1}
Permeability		
darcies	9.870×10^{-13}	m^2
Transmissivity		
U.S. gal day^{-1} ft^{-1}	1.438×10^{-7}	m^2 sec^{-1}
U.S. gal min^{-1} ft^{-1}	2.072×10^{-1}	l sec^{-1} m^{-1}
Magnetic field intensity		
gausses	1.0×10^{5}	gammas
Energy, heat		
British thermal units, BTU	2.52×10^{-1}	calories, cal
BTU	1.0758×10^{2}	kilogram-meters, kgm
BTU lb^{-1}	5.56×10^{-1}	cal kg^{-1}
Temperature		
°C + 273	1.0	°K (Kelvin)
°C + 17.78	1.8	°F (Fahrenheit)
°F − 32	5/9	°C (Celsius)

**Divide by* the factor number to reverse conversions.
Exponents: for example 4.047×10^{3} (see acres) = 4,047; 9.29×10^{-2} (see ft^2) = 0.0929.

Editor: Jiri Zidek

Typeface: Palatino

Presswork: Miehle Single Color Offset
Miller Two-color Offset

Binding: Saddlestitched

Paper: Cover on 12 pt. Kivar
Text on 70 lb white matte

Ink: Cover—PMS 320 Text—Black

Quantity: *1,000*